

1 **Autonomous profiling float observations of the high biomass plume downstream of the**
2 **Kerguelen plateau in the Southern Ocean**

3
4
5 M. Grenier^{1*}, A. Della Penna², and T. W. Trull³

- 6
7 1. Antarctic Climate and Ecosystems Cooperative Research Centre, Hobart, Tasmania, Australia, and Laboratoire
8 d'Etudes en Géophysique et Océanographie Spatiales (CNRS/CNES/IRD/University of Toulouse), Toulouse,
9 France. Now at Earth, Ocean and Atmospheric Sciences (University of British Columbia), Vancouver, Canada.
- 10 2. Quantitative Marine Sciences PhD Program, Institute for Marine and Antarctic Studies, University of
11 Tasmania, and Commonwealth Scientific and Industrial Research Organisation, Hobart, Tasmania, Australia,
12 and Sorbonne Universités, UPMC Univ Paris 06, UMR 7159, LOCEAN-IPSL, F-75005, Paris, France and
13 Univ Paris Diderot Cité
- 14 3. Commonwealth Scientific and Industrial Research Organisation, Oceans and Atmosphere Flagship, Hobart,
15 Tasmania, Australia, and Antarctic Climate and Ecosystems Cooperative Research Centre, Hobart, Tasmania,
16 Australia

17
18 *Corresponding author: melaniegrenier14@yahoo.fr

21 Natural iron fertilisation from Southern Ocean islands results in high primary production and
22 phytoplankton biomass accumulations readily visible in satellite ocean colour observations. These
23 images reveal great spatial complexity with highly varying concentrations of chlorophyll, presumably
24 reflecting both variations in iron supply and conditions favouring phytoplankton accumulation. To
25 examine the second aspect, in particular the influences of variations in temperature and mixed layer
26 depth, we deployed four autonomous profiling floats in the Antarctic Circumpolar Current near the
27 Kerguelen plateau in the Indian sector of the Southern Ocean. Each 'bio-profiler' measured more than
28 250 profiles of temperature (T), salinity (S), dissolved oxygen, chlorophyll-a (Chl-a) fluorescence,
29 and particulate backscattering (b_{bp}) in the top 300 meters of the water column, sampling up to 5
30 profiles per day along meandering trajectories extending up to 1000 km. Comparison of surface Chl-
31 a estimates (analogous to values from satellite images) with total water column inventories revealed
32 largely linear relationships, suggesting that these images provide credible information on total and
33 not just surface biomass accumulations. Regions of very high Chl-a accumulation ($1.5-10 \mu\text{g L}^{-1}$)
34 were associated predominantly with a narrow T-S class of surface waters. In contrast, waters with
35 only moderate Chl-a enrichments ($0.5-1.5 \mu\text{g L}^{-1}$) displayed no clear correlation with specific water
36 properties, including no dependence on mixed layer depth or the intensity of stratification.
37 Geostrophic trajectory analysis suggests that both these observations can be explained if the main
38 determinant of biomass in a given water parcel is the time since leaving the Kerguelen plateau. One
39 float became trapped in a cyclonic eddy, allowing temporal evaluation of the water column in early
40 autumn. During this period, decreasing surface Chl-a inventories corresponded with decreases in
41 oxygen inventories on sub-mixed layer density surfaces, consistent with significant export of organic
42 matter ($\sim 35\%$) and its respiration and storage as dissolved inorganic carbon in the ocean interior.
43 These results are encouraging for the expanded use of autonomous observing platforms to study
44 biogeochemical, carbon cycle, and ecological problems, although the complex blend of Lagrangian
45 and Eulerian sampling achieved by the floats suggests that arrays rather than single floats will often

46 be required, and that frequent profiling offers important benefits in terms of resolving the role of
47 mesoscale structures on biomass accumulation.

48 **1 Introduction**

49 The productivity of the Southern Ocean is important for many reasons. It supports fisheries and
50 high conservation value marine mammal and bird populations ([Constable et al., 2003](#); [Nicol et al.,
51 2000](#)), influences the carbon dioxide content of the atmosphere ([Sarmiento and Le Quéré, 1996](#);
52 [Sigman and Boyle, 2000](#); [Watson et al., 2000](#)), and affects the magnitude of nutrient supply to large
53 portions of the global surface ocean ([Sarmiento et al., 2004](#)). This productivity is limited by the scarce
54 availability of iron (Fe) as an essential micro-nutrient ([Boyd and Ellwood, 2010](#); [Boyd et al., 2007](#);
55 [Martin, 1990](#)). Island sources of Fe elevate productivity and produce downstream 'plumes' of elevated
56 phytoplankton biomass that contrasts with the general HNLC (High Nutrients, Low Chlorophyll)
57 nature of the Southern Ocean ([Blain et al., 2007](#); [de Baar et al., 1995](#); [Mongin et al., 2009](#); [Pollard et
58 al., 2009](#); [Nielsdóttir et al., 2012](#)). Ship based studies of several of these regions, focused on the
59 influence of Fe on carbon (C) transfer to the ocean interior ([Blain et al., 2008](#); [Salter et al., 2007](#)),
60 have revealed a diversity of responses in terms of intensity of enhanced productivity, biomass
61 accumulation, and ecosystem structures. This diversity derives from interactions between the supply
62 and bio-availability of iron with other drivers of productivity such as temperature, water column
63 stratification and stability, light levels, and the possibility of co-limitation by other nutrients ([Assmy
64 et al., 2013](#); [Boyd et al., 1999, 2001](#); [Queguiner, 2013](#)).

65 Assessing influences on productivity, biomass accumulation, carbon export, and carbon dioxide
66 (CO₂) uptake in the Southern Ocean is challenging because of variations across many scales,
67 including weather, seasonal, and interannual time-scales, and sub-mesoscale, mesoscale, and
68 circumpolar frontal space scales ([Joubert et al., 2014](#); [Le Quéré et al., 2010](#); [Lenton et al., 2013](#); [Levy,
69 2003](#); [Nicol et al., 2000](#); [Shadwick et al., 2015](#); [Sokolov and Rintoul, 2007](#); [Swart et al., 2014](#);
70 [Thomalla et al., 2011](#); [Weeding and Trull, 2014](#)). Satellite observations offer extensive space-time
71 coverage ([Martinez et al., 2009](#); [Moore and Abbott, 2000](#)), but may provide a biased view if surface
72 distributions are not representative of water column inventories. Important ways that bias could arise
73 include lack of direct correlations of surface values with their vertical extents (e.g. high surface

74 chlorophyll values might be predominantly associated with shallow accumulations, through the
75 promotion of production by higher light levels in shallow mixed layers; [Sverdrup, 1953](#)), the presence
76 of unobserved subsurface chlorophyll maxima ([Carranza et al., 2014](#); [Schlitzer, 2002](#)), or the variation
77 of phytoplankton to chlorophyll ratios with growth conditions ([Cloern et al., 1995](#); [Fennel and Boss,](#)
78 [2003](#); [Goericke and Montoya, 1998](#)).

79 These difficulties of observation become even more acute for carbon export estimates, which
80 require either flux measurements (e.g. from moored or free-drifting sediment traps or radionuclide
81 activities ([Planchon et al., 2014](#); [Savoie et al., 2008](#)) or the partitioning of changes in state variables
82 across biogeochemical versus oceanographic causes (e.g. nitrate depletions in surface waters or
83 oxygen consumption at mesopelagic depth; [Matear et al., 2000](#); [Trull et al., 2015](#)). Obtaining
84 estimates of carbon export and the depth of its penetration into the ocean interior are important to
85 determining impacts on the climate system, because variations in these two factors have similar
86 influence to variations in total primary production in terms of the sequestration of CO₂ from the
87 atmosphere ([Boyd and Trull, 2007](#)). Notably, export estimates expressed as ‘e-ratio’ fractions of
88 primary production ([Maiti et al., 2013](#)), or as ‘f-ratio’ fractions of production derived from ‘new’
89 nitrate supply ([Savoie et al., 2004](#)) vary widely in the Southern Ocean, with the possibility that these
90 efficiencies are increased by natural iron fertilisation ([Jouandet et al., 2011](#); [Trull et al., 2008](#)).

91 This space-time complexity is abundantly demonstrated by the 'mosaic of blooms' (i.e. patchiness
92 pattern) encountered in waters downstream from the Kerguelen plateau during the KEOPS2 field
93 program in austral spring (October-November 2011), as detailed in many papers in a special volume
94 of Biogeosciences ([d’Ovidio et al., 2014](#); [Trull et al., 2015](#); [Lasbleiz et al., 2014](#); [Laurenceau-Cornec](#)
95 [et al., 2015](#); [Cavagna et al., 2014](#)). Much of the meso-scale spatial variations in biomass accumulation,
96 as seen in satellite images and animations ([Mongin et al., 2009](#); [d’Ovidio et al., 2014](#); [Trull et al.,](#)
97 [2015](#)), appears to result from the interleaving of iron-enriched water parcels that have transited the
98 Kerguelen plateau with surrounding iron poor waters, as demonstrated by analysis of satellite

99 altimetry based circulation estimates and surface drifter trajectories ([Park et al., 2014a](#); [d'Ovidio et](#)
100 [al., 2014](#)). However, shipboard studies close to the plateau ([Mosseri et al., 2008](#); [d'Ovidio et al., 2014](#);
101 [Blain et al., 2015](#); [Trull et al., 2015](#); [Lasbleiz et al., 2014](#); [Laurenceau-Cornec et al., 2015](#)) suggest
102 that other factors are also likely to play a role, including mixed layer depth and upper water column
103 stratification.

104 To explore the influence of variations in these water column properties on bloom structure at
105 larger scale, in particular further from the plateau than could be surveyed by ship, we deployed
106 autonomous profiling drifters. The first one was successfully launched during the KEOPS2 field
107 program in late October 2011, and the other three during the MyctO-3D-MAP (referred to as
108 MYCTO, from now on in this text) interdisciplinary survey between late January and early February
109 2014. Given the extent of the Kerguelen biomass plume (> 1000 km; [Mongin et al., 2009](#)), the
110 remoteness from ports, and the generally rough sea states, the use of autonomous platforms is
111 arguably the only affordable way to survey this region. As shown in Figure 1, these deployments
112 returned data from a large proportion of the enriched biomass plume downstream of the Kerguelen
113 plateau.

114 In this paper, we use the bio-profiler observations to address three questions:

- 115 1) Do satellite images of surface chlorophyll provide an unbiased guide to the spatial distribution
116 of total water column chlorophyll, or are they biased by lack of knowledge of variations in the
117 vertical extent of chlorophyll distributions or the presence of subsurface chlorophyll maxima?
- 118 2) Do regions of high biomass correlate with particular oceanographic properties, such as warmer
119 or fresher waters, or the intensity of stratification? If so, are these properties determined locally
120 or by the upstream origins of the different water parcels?
- 121 3) Can the fate of surface enrichments in biomass be determined (and eventually quantified) from
122 along-trajectory temporal variations in biogeochemical properties, for example by progressive

123 downward movement of fluorescence or particulate backscattering signals or decreases of
124 oxygen in subsurface waters?

125

126 **2 Methods**

127 **2.1 Float sensor and mission configurations**

128 The float deployment locations are provided in Table 1, along with their identification numbers
129 which provide access to their full data sets via the Australian Integrated Marine Observing System
130 (www.imos.org.au). Float deployment was done in 2011 by manual transfer to a small boat and then
131 the sea, and in 2014 by deploying the floats from the ship deck inside cardboard boxes designed to
132 readily disintegrate after release. The autonomous profiling floats were all of the same design (Model
133 APF9I, Teledyne-Webb, Inc.). Each was equipped with pumped, poisoned, thermosalinographs
134 (Model SBE 41CP-2.0, Seabird, Inc.), end-cap mounted un-pumped oxygen optodes (Model 3830,
135 Aanderaa, Inc.), and two-channel bio-optical sensors (Model FLBBAP2, Wetlabs, Inc.) strapped onto
136 the lower third of the float hull with their optical ports facing horizontally to minimize possible
137 interferences from particle accumulation. Owing to the structure of the firmware for the floats and
138 the varying power requirements for the sensors, the sampling rates differed for the physical and
139 biogeochemical parameters. Temperature and salinity were sampled at the highest rates, yielding
140 values at 2 decibar intervals (used in this work as equivalent to 2 meter depth intervals without density
141 corrections), whereas oxygen, fluorescence and backscatter were sampled at 10 decibar intervals,
142 except for bio-profiler #1 where they were sampled at 5 decibar intervals in the first 150 m.

143 Temperature and salinity calibrations were performed by Seabird, Inc., with estimated accuracy
144 and precision of better than 0.005 °C and 0.01, respectively ([Oka and Ando, 2004](#)). These variables,
145 used as water mass proxies and to estimate mixed layer depths and stratification intensity (expressed
146 as the Brunt-Väisälä frequency), helped to determine if dissolved oxygen evolutions were mainly due

147 to physical processes or to biological production or respiration processes. The oxygen optodes were
148 calibrated at CSIRO prior to mounting on the floats against a 20 point matrix of 4 temperatures (0.5
149 - 30) and 5 oxygen saturations (0 - 129%) using the methods detailed in [Weeding and Trull \(2014\)](#).
150 Similar sensors exhibited drift during a 6 month mooring deployment in the Southern Ocean of less
151 than $1.7 \mu\text{mol kg}^{-1}$ over 6 months ([Weeding and Trull, 2014](#)).

152 The bio-optical sensors measured chlorophyll-a fluorescence via stimulation/emission at 470/695
153 nm) and particulate backscattering at 700 nm. Chlorophyll-a fluorescence is a useful proxy for
154 chlorophyll-a concentration and standing stocks of phytoplankton biomass ([Falkowski and Kiefer,
155 1985](#); [Huot et al., 2007](#)). Particulate backscattering provides a good proxy for particulate organic
156 carbon ([Stramski et al. 2008](#); [Cetinić et al, 2013](#)). The bio-optical fluorescence sensors were calibrated
157 (by the manufacturer, Wetlabs, Inc.) against fluorescent uranine solutions as working standards, and
158 cross-referenced to prior measurements of a laboratory culture (25 mg m^{-3} chlorophyll) of the diatom
159 *Thalassiosira weissflogii* to yield chlorophyll estimates. These calibrations are warranted to yield
160 linear responses with precisions among multiple sensors of better than 10%, and (after one cycle of
161 testing and replacement with the manufacturer) we obtained reproducibility for the set of three floats
162 deployed in 2014 of better than 4% based on measurements with fluorescent and non-reflective
163 plastics ([Earp et al., 2011](#)). Accordingly, calculation of the chlorophyll fluorescence from the float
164 data was done by removal of the background dark signals measured prior to deployment and scaling
165 to chlorophyll using the manufacturer's calibrations. Similarly, the retrieval of particulate
166 backscattering, b_{bp} (m^{-1}), at 700 nm from the backscatter raw transmitted measurement (counts) was
167 done by applying the manufacturer-provided scaling factor after correction for dark counts (i.e.
168 measured signal output of the backscatterometer in clean water with black tape over the detector),
169 with the additional steps of removal of the pure seawater backscattering contribution ([Zhang et al.,
170 2009](#)), and scaling from the limited solid angle sensor measurement to the total backscattered
171 hemisphere based on relations estimated from observations for a wide range of marine particles ([Boss
172 and Pegau, 2001](#); [Sullivan et al., 2012](#)).

173 In contrast to typical Argo program float missions for climate studies (www.argo.org), which
174 consist of deep (2000 m) profiles every 10 days, the bio-profilers were programmed to focus on the
175 upper water column and carried out continuous profiling between the surface and 300 m depth,
176 achieving 4 to 6 profiles per day, depending on the stratification. This temporal resolution was
177 intended to allow examination of daily cycles related to insolation, photosynthesis, and respiration.
178 In practice, it proved difficult to extract clear cycles because of aliasing from spatial variations.
179 Consequently, after several weeks for the 2011 KEOPS2 deployment of bio-profiler #1, the frequency
180 of profiles was reduced to twice daily, to provide extended battery life while still obtaining night and
181 day observations to allow insolation quenching of the fluorescence response to be evaluated and
182 corrected, and thus to avoid inappropriate inference of subsurface chlorophyll maxima from the
183 fluorescence signal ([Sackmann et al., 2008](#); [Xing et al., 2012](#)). For bio-profilers #2, #3, and #4
184 deployed in 2014, the missions were further refined, via automated telemetric switching of mission
185 configuration files, to carry out a deep profile to ~1500 m every 3 days to provide deep reference
186 points for temperature, salinity, and oxygen observations, and also with the intention to slow the
187 development of bio-fouling of the bio-optical sensors by exposing surface organisms to high
188 pressures.

189

190 **2.2 Float data quality control**

191 Extensive experience by the Argo program with profiling float measurements for temperature
192 (T) and salinity (S), including recovery of floats for post deployment tests ([Oka and Ando, 1994](#)),
193 suggests that these sensors reliably deliver accurate and precise observations (to better than 0.005 °C
194 and 0.01 salinity) over multi-annual deployments. Given our much shorter bio-profiler deployments
195 (3 to 6 months) and their observed T-S relationships which fall within those of the ship-based
196 KEOPS2 observations, we assume these variables are correct and make no further assessment or

197 correction. We similarly accept the oxygen observations, given our careful attention to their pre-
198 deployment calibration, their reasonable range of surface water oxygen super-saturations (96-103%
199 for low chlorophyll waters and extending up to 108% in correlation with very high chlorophyll waters,
200 as discussed further below), and their deep ocean values (950-1000 m depths) which fall within the
201 range of nearby ship observations and showed no temporal trends and standard deviations of less than
202 $4 \mu\text{mol kg}^{-1}$ over the deployment periods (ranging from 1 to $3.9 \mu\text{mol kg}^{-1}$ for the four bio-profilers).

203 To evaluate the possibility of temporal sensor drifts in bio-optical variables, we examined the
204 variations of the bio-optical variables in mesopelagic (250-300 m) and deep water (950-1000 m)
205 values, i.e. at depths where little signal was anticipated and most profiles reached steady background
206 values (Figure 2a). The particulate backscattering and, to a lesser extent, the Chl-a fluorescence
207 signals showed spikes which presumably reflect larger particles such as aggregates and zooplankton,
208 motivating our examination of average values over 50 m ranges (250-300 m and 950-1000 m depth
209 layers) for the assessment of temporal drifts. As shown in Figure 2a and quantified in Table 2, for
210 most of their deployment periods all four bio-profilers exhibited no significant temporal drift of these
211 deep values except for bio-profiler #1, for which high and erratic values of Chl-a and b_{bp} began to
212 occur after profile #300 both at depth (Figure 2a) and throughout the water column (Figure 3.1c and
213 e). We consider this to be caused by bio-fouling and do not use this data in any subsequent analysis
214 (this loss of signal fidelity was one of the motivations for including periodic deep profiles in the
215 subsequent three bio-profiler deployments, as a means of retarding fouling). In contrast, the high
216 fluorescence chlorophyll values found in mesopelagic waters from profiles ~#100 to ~#170 along the
217 bio-profiler #1 trajectory appear to be real and to reflect the deep extension of high biomass
218 occurrence at this time, as discussed further below (see also Figure 3.1c). Consequently, this range of
219 profile was not taken into account for the drift calculation in Table 2. Overall, except for the bio-
220 profiler #1, most of the bio-optical sensors showed a slight loss of sensitivity with time, as indicated
221 by the negative slopes of the trend of their responses in the two considered depth layers (Table 2).
222 Over the time course of the bio-optical sensor observations, these sensor drifts were small in

223 comparison to the changes observed for surface bio-optical values, contributing less than 7% to either
224 fluorescence or particulate backscattering. The only exception was the drift for the bio-profiler #2 b_{bp}
225 sensor in the 250-300 m layer, where drift appeared to have been larger (though of course changes at
226 this depth range may also be oceanic) and reached up to 19 % of the low surface b_{bp} values for this
227 bio-profiler.

228 Fluorescence signals were also corrected for daytime quenching. This effect, which derives from
229 the photo-inhibition of phytoplankton by an excess of light (maximum at midday), decreases surface
230 fluorescence ([Falkowski and Kolber, 1995](#); [Kiefer, 1973](#)) and, if uncorrected, can produce a false
231 impression of subsurface maxima in fluorescence derived chlorophyll profiles. We explain this
232 correction and its evaluation in considerable detail in the following paragraphs, but note that none of
233 the conclusions of the paper depend on these corrections because the same overall results are obtained
234 if we use only Chl-a fluorescence signals collected at night. Our purpose in detailing the correction
235 is to contribute to active discussion of the best way to use daylight Chl-a fluorescence data obtained
236 from platforms which may not have as good night time coverage as our floats (such as sensors
237 deployed on seals, on standard ARGO 10- day profile interval missions, or on float missions that
238 target co-measurement with daytime satellite ocean colour observations).

239 We defined the daytime profiles, potentially affected by quenching, as profiles acquired between
240 one hour after local sunrise time and one hour after local sunset time, to allow for dark acclimation
241 since quenching effect could still persist after sunset ([Sackmann et al., 2008](#)). Daytime profiles from
242 the four bio-profilers are shown to illustrate this effect (continuous lines in Figure 2b, left panel). To
243 correct this bias, we applied the method of [Sackmann et al. \(2008\)](#), which uses the particulate
244 backscattering signal as a relative reference. For the sake of consistency with the other studies of this
245 issue, we defined the mixed layer depth, MLD, as the depth where density increased by 0.02 kg m^{-3}
246 relative to the density at 10 m ([Park et al., 1998](#)). Within the deeper half of the mixed layer (targeted
247 to be below the depth of daytime quenching), we determined a mean value of the (relatively constant,

248 see below) Chl-a fluorescence to b_{bp} ratio (at depth defined as $d_{F/b_{bp}}$) and multiplied this ratio by the
249 b_{bp} signal at this depth to retrieve the Chl-a fluorescence. Then, we multiplied this same ratio by the
250 surface b_{bp} value to estimate unquenched surface Chl-a fluorescence, and interpolated between these
251 two depths to obtain the unquenched Chl-a fluorescence profile. This assumes that phytoplankton
252 populations were not stratified within the density defined mixed layer. This works particularly well
253 for deep mixed layers (>50 m) which exhibit relatively constant Chl-a fluorescence/ b_{bp} ratios (to
254 within $\sim 10\%$) in their deeper half. In less than 3% of the daytime profiles, in average, we could not
255 identify a region of uniform Chl-a fluorescence/ b_{bp} and apply the quenching correction; consequently,
256 these profiles were not used further.

257 The greater spikiness of the b_{bp} profiles in comparison to those of fluorescence (as illustrated in
258 Figure 2b, right panels) means that this quenching correction introduces some noise into the daytime
259 chlorophyll estimates. In principle, this could be filtered or smoothed, but the low 10 m vertical
260 resolution of the observations made this rather uncertain and so we have used the unfiltered
261 observations throughout this paper (except in Figure 9f below where we show median-filtered
262 particulate backscattering profiles for the sake of visual clarity). Note that to avoid to correct the
263 surface Chl-a fluorescence with a spiked surface b_{bp} value and create a “ b_{bp} spiked” interpolation, we
264 verified before that the b_{bp} surface value did not seem to be spiked, assuming that surface value should
265 not exceed more than $\pm 50\%$ of the b_{bp} value at the depth $d_{F/b_{bp}}$, since within the mixed layer. This
266 threshold was defined after assessing the backscatterometer precision (using the coefficient of
267 variation of b_{bp} , i.e. the ratio of the standard deviation to the mean) between 500 and 1000 m depth of
268 $14 \pm 4\%$ in average. If the surface b_{bp} value was considered as spiked (less than 4% of the daytime
269 b_{bp} profiles, except for bio-profiler #4 for which it reached 9%), the test was done with the second
270 depth value, until a “non-spiked” value was found, and the value was then extrapolated to the surface.

271 The effects of the quenching correction on our selected chlorophyll profiles are shown in Figure
272 2b (middle panels, continuous lines), and summary statistics for all the profiles are provided in Table
273 3. Without the correction, on average, more than 70% of the daytime profiles exhibited a subsurface

274 maximum exceeding 60% of the surface value –defined after assessing the fluorometer error
275 (coefficient of variation of Chl-a concentration) between 250 and 300 m depth and between 500 and
276 1000 m depth of $22 \pm 10\%$ in average. After applying the quenching correction method, the number
277 of daytime profiles exhibiting a subsurface maximum exceeding 60% of the surface value was
278 reduced to very similar levels to those observed in the night time profiles, although slightly higher
279 (of 21% in average), indicating, with the fact that these daytime subsurface maxima occurred mostly
280 below the MLD, that the correction was largely successful. Notably, for the total data set, after
281 quenching correction, less than 11% of the profiles exhibited a deep maximum exceeding 100% of
282 the surface value (Table 3), and these profiles were primarily located in a restricted region near the
283 Gallieni Spur, as discussed further in the Results section.

284 Even after our quenching correction, 10% of the corrected daytime profiles (in average for all 4
285 bio-profilers) still exhibited significant decrease of the Chl-a fluorescence in the surface layer. We
286 were not able to conclude if these decreases were due to an incomplete quenching correction or if
287 they were true features, given that $\sim 14\%$ of the night profiles in average exhibited subsurface values
288 at least 60% higher than the surface values. Consequently, we defined a threshold surface value for
289 each bio-profiler, defined as a slightly lower value than the minimum surface value reached during
290 night profiles (see squares in Figure 2b, middle panel, and caption) and we flagged all the corrected
291 daytime profiles that had a surface value lower than this threshold as potentially arising from
292 incomplete correction of quenching. These distinctions between night, daytime and flagged profiles
293 are illustrated in Figures 4, 5 and 7, and further discussed in the Results and Discussion sections
294 below. Note that, using a different quenching correction method, [Biermann et al. \(2015\)](#) recently
295 observed similar features and statistics in fluorescence profiles collected by southern elephant seals
296 during austral summer in the vicinity of Kerguelen Island.

297 Finally, we emphasize that the bio-optical measures of chlorophyll and particulate backscattering
298 are based on laboratory calibrations that are not specific to Southern Ocean phytoplankton or particle

299 properties. This means that while interpretation of local variations is reasonably straightforward,
300 quantitative comparisons to other observations much more uncertain (except perhaps in the future for
301 other serial numbers of these sensors, calibrated in the same limited way). For the 3 bio-profilers
302 deployed in 2014, no ancillary shipboard measurements are available to evaluate this issue, but in
303 2011 some chlorophyll samples were collected by the KEOPS2 science team that allow for limited
304 evaluation of the bio-profiler #1 calibration.

305 Bioprofiler #1 was deployed into a semi-permanent meander of the Polar Front, which the
306 KEOP2 program examined as a Lagrangian time series following surface drifters. As shown in Figure
307 2c, the first and second stations in the meander (E1 CTD-27 on 29 October 2011 at 22:46 local time
308 and E2 CTD-43 on 1 November 2011 at 12:00 local time) bracketed the locations of the first 11
309 autonomous bio-profiler #1 profiles (Figure 2c.i). The bio-profiler #1 temperature profiles are
310 intermediate between the ship results (Figure 2c.ii), with the variations in temperature profiles mainly
311 driven by vertical motions associated with internal waves ([Park et al., 2014b](#)). In Figure 2c.iii, the
312 KEOPS2 shipboard fluorescence results are displayed after linear calibration to high pressure liquid
313 chromatography (HPLC) total chlorophyll-a results from below 40 meters depth (below the depth of
314 non-photochemical quenching). The data reveal two important features: i) good fits achieved below
315 40 meters do not extend to the surface – where fluorescence/chlorophyll-a ratios were higher than at
316 depth, apparently as a result of community composition variations with depth (see also [Lasbleiz et al.](#)
317 [2014](#)), and ii) the bio-profiler #1 fluorescence data displayed similar characteristics and good accord
318 with the shipboard results. In light of the limited available data, a non-linear calibration of
319 fluorescence to chlorophyll-a was not pursued, and no adjustments were made to the laboratory bio-
320 profiler calibration.

321 These variations in fluorescence/chlorophyll-a ratios within individual CTD casts in the
322 shipboard observations serve as a strong reminder that fluorescence is an imperfect proxy for
323 chlorophyll-a concentrations, owing to variations with phytoplankton community structure,
324 physiology, and other effects (e.g. [Babin et al., 1996](#); [Cullen, 1982](#); [Suggett et al., 2011](#)). Thus,

325 interpretation of our sensor records, as with any bio-optical sensor results, must keep this in mind and
326 avoid over-interpreting small variations in fluorescence as necessarily resulting from variations in
327 chlorophyll or phytoplankton biomass.

328 **2.3 Satellite data sources**

329 We used satellite products to provide physical and biological context for the bio-profiler
330 trajectories, including the effectiveness of their sampling of high biomass waters downstream of
331 Kerguelen. The images of surface chlorophyll concentrations shown in Figure 1 to provide context
332 for the plume sampling achieved by the bio-profilers are the CLS SSALTO/DUACS 4 km daily
333 product derived from NASA MODIS-Aqua observations (Figure 1), without modification for recent
334 suggestions that this algorithm may underestimate chlorophyll in low chlorophyll waters south of
335 Australia ([Johnson et al., 2013](#)).

336 To better understand the observed bio-profiler trajectories, we calculated expected movements
337 based on geostrophic currents estimated from satellite altimetry using the multi-satellite global
338 product Delayed Time Maps of Absolute Dynamic Heights (DT-MADT) developed by the
339 CNES/CLS Aviso project (www.aviso.oceanobs.com). This product has 1 week temporal and 1/3°
340 spatial resolutions, and was used to compute Lagrangian trajectories to produce a diagnostic for eddy
341 retention ([d'Ovidio et al., 2013](#); Figure 9b) and water origin and age ([d'Ovidio et al., 2014](#); Figure 8).
342 Eddy retention is a measure of how much time a synthetic water parcel has been recirculating within
343 an eddy core. Long-lived and coherent eddies are characterised by water parcels with high values of
344 retention (measured in days since a water parcel has been entrained by an eddy), whereas recently
345 formed eddies or eddies that exchange strongly with surrounding regions have low retention values.
346 Following [d'Ovidio et al. \(2014\)](#) and [Sanial et al. \(2014\)](#), we used back-tracking of virtual water
347 parcels (from the bio-profiler profile locations) to compute how long ago (water age) and at which
348 latitude (water origin) the sampled parcels had been in contact with the Kerguelen Plateau (defined

349 as the 700 m isobath, as shown in red in Figure 3.1). Figure 8 a) and c), adapted from [d'Ovidio et al.](#)
350 [\(2014\)](#), display example maps of the calculated daily snapshots of these water ages and water origins.
351 For each pixel in these maps, virtual water parcels were back tracked for 90 days. They are shown as
352 white pixels on the maps if during that time they never touched the Kerguelen Plateau (shown in grey
353 on the map), and otherwise are coloured for the time between the contact with the plateau and the day
354 of the map computation (water age, Figure 8a) and the latitude of the last contact with the plateau
355 stored (water origin, Figure 8c). These same computations were performed for each location sampled
356 by the bio-profilers, in order to compare the water ages and origins with their measured chlorophyll
357 inventories.

358

359 **3 Results**

360 **3.1 Coverage of the plume**

361 The drifts of the bio-profilers provided coverage of a large portion of the elevated biomass plume
362 (Figure 1), from near the Kerguelen plateau to more than 700 miles downstream (71 to 95° E) and
363 nearly 400 miles from north to south (47.5 to 54° S), thereby spanning waters of the Polar Frontal
364 and Antarctic Zones ([Orsi et al., 1995](#); [Park et al., 2008b](#); [Sokolov and Rintoul, 2009](#)). Unfortunately,
365 this breadth of spatial coverage of the plume did not extend to full temporal seasonal coverage, and
366 this is important to keep in mind given the strong seasonal cycle of biomass accumulation ([Trull et](#)
367 [al., 2015](#); [Blain et al., 2007](#); [Mongin et al., 2008](#)). As shown in these images, the 2011 bio-profiler
368 covered the period of highest biomass accumulation, while the 2014 deployments occurred after this
369 seasonal peak, and thus sampled the system during its senescence (to illustrate these prior conditions,
370 Figure 1 also includes biomass distribution images from late 2013, before the launch of the three bio-
371 profilers in early 2014). Thus, the profilers obtained some seasonal context for the central portion of
372 the plume (which was sampled well in 2011 by bio-profiler #1 in spring and summer and again by
373 bio-profilers #2 and #3 in summer and autumn). However, sampling of the north-eastern portion of

374 the downstream plume (north of the Polar Front) was achieved only in late summer and autumn (by
375 bio-profiler #4).

376 Bio-profiler #1 in spring 2011 and bio-profiler #3 in 2014 were deployed in the centre of the
377 quasi-stationary cyclonic recirculation just east of the northern Kerguelen plateau ([d'Ovidio et al.,
378 2014](#); [Park et al., 2014a](#)). Both bio-profilers exited this region to the northeast, tracking towards the
379 Gallieni Spur, before transiting strongly southward near 74° E. This southward transport has also
380 been observed for surface drifters and appears to be associated with a persistent meander of the Polar
381 Front ([d'Ovidio et al., 2014](#); [Park et al., 2014a](#)). Thus bio-profilers #1 and #3 provide spring and
382 summer perspectives respectively for these portions of the biomass plume (albeit in different years).

383 Bio-profiler #2 was deployed further south, close to the region where the strong north to south
384 transport portions of the bio-profilers #1 and #3 trajectories finished. Thus bio-profiler #2 provided
385 some overlap with the southern portion of the bio-profiler #1 trajectory, before being carried the
386 furthest south, where it explored cold waters close to the Williams Ridge that extends to the southeast
387 of Heard Island and terminates near the Fawn Trough (a gap in the plateau which permits the passage
388 of much of the deep water eastward transport; [Park et al., 2008b](#); [2014a](#)). Waters in this region tend
389 to exhibit archetypical high-nutrient, low-chlorophyll characteristics, and were used as a reference
390 station for iron non-fertilised waters during the KEOPS field program in 2005 ([Blain et al., 2007](#);
391 [2008](#)).

392 In contrast, bio-profiler #4 was deployed at similar latitude to bio-profilers #1 and #3, but further
393 east, in particular east of the southward meander of the Polar Front which carried these others to the
394 south. Bio-profiler #4 remained in the northern portion of the plume throughout its deployment,
395 drifting to the northeast roughly parallel to the shallow Eastern Kerguelen Ridge before becoming
396 trapped in a cyclonic eddy in which it obtained a time series of ~100 profiles (as discussed in detail
397 below).

399 3.2 Overview of observed oceanographic properties

400 The bio-profilers return a large number of water column observations making visualisation at the
401 scale of individual profiles only possible for targeted issues. The simplest first-order assessment is
402 most easily done by presenting the results as along-trajectory sections. These are shown for all the
403 observed variables for each bio-profiler in Figures 3.1, 3.2, 3.3 and 3.4, and briefly described in the
404 following paragraphs.

405 Bio-profiler #1, launched in late October 2011 in the centre of the deep water recirculation just
406 east of Kerguelen Island, initially encountered cold, well oxygenated waters with moderate biomass
407 ($T \sim 3 \text{ }^\circ\text{C}$, $\text{O}_2 \sim 330 \text{ } \mu\text{mol kg}^{-1}$, $0.5 \text{ } \mu\text{g L}^{-1} < \text{Chl-a} < 2 \text{ } \mu\text{g L}^{-1}$; profiles 1-90, Nov.). It was then carried
408 north-eastward across the Gallieni Spur where it encountered warmer waters with extremely high
409 biomass ($T \sim 5 \text{ }^\circ\text{C}$, chlorophyll up to nearly $10 \text{ } \mu\text{g L}^{-1}$), which satellite ocean colour animations
410 suggest was being swept northward as a mix of waters from the northern and central regions of the
411 Kerguelen plateau (see the animation “bloom 2011” in supplementary material; [Trull et al., 2015](#)).
412 During the subsequent southward transport, it crossed the Polar Front near 51.5° S , as shown by the
413 presence of a temperature minimum near 150 m depth ($T \sim 1 \text{ }^\circ\text{C}$; profiles ~ 200 -220, end of Jan.).
414 The shoaling of low dissolved oxygen layers in this region provides another indication of their
415 Antarctic Zone oceanographic classification. Surface waters above this remnant winter water were
416 relatively warm despite deep mixed layer depths ($\sim 100 \text{ m}$, $T > 6 \text{ }^\circ\text{C}$; profiles ~ 240 -330, Feb.-Mar.).
417 Much of this warming is probably seasonal, as these waters were encountered in late summer, but the
418 co-occurrence of somewhat elevated salinity (~ 33.8) suggests that flow of Polar Frontal Zone surface
419 waters over the Antarctic waters was also involved. During the February bio-profiler transit, these
420 waters exhibited only low to moderate chlorophyll biomass ($\sim 1.5 \text{ } \mu\text{g L}^{-1}$), although satellite images
421 suggest higher concentrations ($\sim 3 \text{ } \mu\text{g L}^{-1}$) were present earlier in December and January (see Figures
422 1b and 1c and the animation “bloom 2011” in supplementary material; [Trull et al., 2015](#)). The

423 particulate backscattering signal reflected the chlorophyll evolution along most of the trajectory,
424 except in January when, as the chlorophyll levels decreased (from $>3 \mu\text{g L}^{-1}$ to $\leq 2 \mu\text{g L}^{-1}$), b_{bp}
425 remained high and constant ($-2.5 \text{ m}^{-1} \leq \log(b_{bp}) \leq -2.0 \text{ m}^{-1}$), suggesting detrital particles developed
426 from the high chlorophyll biomass, or possibly a (relatively large) change in chlorophyll/particulate
427 organic carbon ratio (Chl/POC) due to phytoplankton community composition. Finally, after 300
428 shallow profiles, bio-fouling of the fluorescence and particulate backscattering sensors marked the
429 end of their utility, as shown by the occurrence of elevated and highly noisy values throughout the
430 water column (see Figure 3.1c and e).

431 Bio-profiler #2, launched in late January 2014 south and east of the recirculation feature, initially
432 encountered Polar Frontal Zone waters which were present further south in this region than during
433 the 2011 year sampled by bio-profiler #1. For approximately the first 150 profiles, these waters
434 displayed relatively homogenous, moderately warm temperatures (4-5 °C) that continued to warm to
435 ~ 6 °C through February. The bio-profiler then transited much further south, briefly encountering
436 waters with strong shoaling of subsurface salty, low oxygen characteristics around profiles 160-170
437 ($S \sim 34.0\text{-}34.2$, $O_2 \sim 260 \mu\text{mol kg}^{-1}$), and entered colder Antarctic waters where it remained through
438 profile ~ 220 , at which time its return north brought it back into Polar Frontal Zone waters showing
439 autumn cooling. Throughout its life, in comparison to bio-profiler #1, only low-to-moderate biomass
440 waters were encountered ($<1.5 \mu\text{g L}^{-1}$), though these values were persistently above Southern Ocean
441 HNLC background values ($< 0.5 \mu\text{g L}^{-1}$). Within this range, the higher biomass values, which also
442 extended over greater vertical extents ($\sim 100 \text{ m}$), were found in the Antarctic waters (profiles 170-
443 250, Mar.-Apr.). In contrast, the higher b_{bp} values were found at the beginning of the trajectory
444 ($\log(b_{bp}) \sim -2.5 \text{ m}^{-1}$), and their deep extent and high values compared to chlorophyll levels suggest
445 the existence of higher chlorophyll concentrations prior to the bio-profiler deployment. This is in
446 agreement with satellite ocean colour animations on which high biomass development is observed in
447 December 2013 in the area of the bio-profiler deployment (see Figures 1e and 1f and the animation

448 “bloom 2013” in supplementary material). After this initial difference, the b_{bp} variations followed
449 those of chlorophyll along the rest of the trajectory.

450 Bio-profiler #3, launched in late January 2014 in the northern portion of the recirculation feature,
451 followed a similar trajectory to that of bio-profiler #1 launched in October 2011 and encountered
452 much warmer waters with similar mixed layer depths, between 40 and 70 m (Figure 3.3). Presumably
453 this represents seasonal warming as salinities were similar to those encountered in spring (~ 33.85),
454 and the warming from ~ 3 °C to nearly 6 °C is consistent with seasonal warming amplitudes observed
455 in satellite surface temperature records for unfertilized open ocean Polar Frontal Zone waters ([Trull
456 et al., 2001](#)). Persistent high chlorophyll levels were also observed initially in the recirculation region
457 (up to ~ 4 versus ~ 1 $\mu\text{g L}^{-1}$), but the float did not cross the Gallieni Spur (GS in maps of Figure 3)
458 where bio-profiler #1 encountered values up to nearly 10 $\mu\text{g L}^{-1}$. During its transit south near 75° E,
459 only Polar Frontal Zone waters were encountered, and chlorophyll levels remained moderately high
460 (between 1 and 2 $\mu\text{g L}^{-1}$). At the beginning of the trajectory, the particulate backscattering b_{bp} signal
461 evolved in concert with the chlorophyll signal, but with a ~ 7 -10 day delay. Another difference
462 between the two biomass parameter evolutions was the large increase of b_{bp} compared to chlorophyll
463 between the surface and 100 m, right after the profiler turned southward in the vicinity of the Gallieni
464 Spur (\sim profiles 190-205, end of March).

465 Bio-profiler #4, deployed well east of the recirculation feature in early February, was initially in
466 warm, quite salty and well oxygenated waters, characterized by moderate biomass (first 80 profiles:
467 $T \sim 5.5$ °C, $S \sim 33.8$, $O_2 \sim 310$ $\mu\text{mol kg}^{-1}$, $\text{Chl-a} < 1.5$ $\mu\text{g L}^{-1}$, $\log(b_{bp}) \sim 3.35$ m^{-1}). As its trajectory
468 approached the Gallieni Spur, surface waters became progressively warmer, fresher and less
469 oxygenated (profiles 80-250: $T \sim 7$ °C, $S \sim 33.7$, $O_2 \sim 290$ $\mu\text{mol kg}^{-1}$). During this time, the bio-
470 profiler recorded high chlorophyll and particle concentrations (chlorophyll values reaching up to 3
471 $\mu\text{g L}^{-1}$ for profiles 80-130). This high biomass could be a remnant of the rich filament that transited
472 in this area a month prior to the visit of the bio-profiler (see the animation “bloom 2013” in
473 supplementary material). As the bio-profiler drifted further east, it was entrained in a relatively

474 stationary cyclonic eddy where it performed several loops before exiting to the south (profiles ~ 130-
475 240, mid-March – mid-April). This eddy can be identified from altimetry as retentive – i.e. capable
476 of entraining Lagrangian particles for, in this case, a few weeks to one month ([d’Ovidio et al., 2013](#);
477 Figure 8b). While retained by this mesoscale eddy, the bio-profiler measured a relatively constant
478 profile of temperature and salinity, with slowly decreasing Chl-a concentrations and b_{bp} (Figure 8).
479 Relatively constant hydrological properties throughout this period and the repeated looping suggest
480 a largely Lagrangian trajectory within a single water parcel at this time. Of all the observations, this
481 region displayed surface waters with the highest temperatures and lowest salinities ($T \sim 8.0$ °C, $S \sim$
482 33.6).

483

484 **4 Discussion**

485 With this overview of the spatial and temporal characteristics of our observations in hand, we
486 proceed to evaluate our research questions.

487 **4.1 Do the satellite images of surface chlorophyll reflect water column contents?**

488 As discussed in the Introduction, it is important to determine whether the water column
489 information provided by the bio-profilers changes perspectives on the mesoscale distributions of
490 chlorophyll as seen in satellite images (Figure 1) This is a larger issue than whether our in-situ
491 measurements of surface values differ from satellite values. We did not evaluate that question owing
492 to extensive cloud cover greatly limiting match-ups between bio-profiler and satellite observations,
493 and because we know that both our sensor calibrations and the satellite algorithms have large
494 uncertainties (see the Methods sections 2.2 and 2.3). Instead, we examined the bio-profiler water
495 column observations to determine what biases might be expected from observing only their upper
496 portions, i.e. as a satellite would. There are two aspects of this issue that we could readily address: i)
497 were subsurface chlorophyll maxima commonly present below the depth of satellite observation, and

498 did they vary spatially or temporally? ii) were surface chlorophyll values linearly and tightly
499 correlated with water column inventories with similar dynamic ranges, or were surface values poor
500 guides to water column inventories? We address these issues in this order in the following paragraphs.

501 Our statistics on the occurrence of subsurface chlorophyll maxima (Table 3) show that these
502 features were present in a significant fraction of the profiles (up to 14% of the night profiles and up
503 to 21% of the quenching-corrected day profiles). They mostly occurred at depths greater than the
504 MLD (Table 3) and, thus, too deep to be taken into account in the satellite observations. Without
505 radiation sensors on the bio-profilers, the first penetration depth (z_{pd} , light attenuation by $1/e$) that
506 characterizes satellite observations could not be directly estimated, but based on the model of [Morel
507 and Maritorena \(2001\)](#); their figure 6), and using the relationship $z_{pd} = z_{eu}/4.6$ for the euphotic zone
508 definition of the 1% photosynthetically active radiation level ([Gordon and McCluney, 1975](#)), it was
509 at most 10-15 meters, and thus always within the mixed layer. Thus, we focused on these subsurface
510 maxima occurring below the MLD (hereafter SubMax_{>MLD}) and we examined the location of the
511 profiles exhibiting these features as well as their associated depth (see Figures 4a, 4b, 4d and 4e).

512 These SubMax_{>MLD} were quite localized. They occurred primarily near the plateau or close to the
513 location of the Polar Front. Specifically, most of the profiles exhibiting this feature were found in the
514 vicinity of the steep slope between the Northern Kerguelen Plateau and the Gallieni Spur, between
515 40 and 80 m depth (Figures 4a, 4b, 4d and 4e). Occurrences of SubMax_{>MLD} were much more sporadic
516 south of 50° S, on the south-eastward trajectories of bio-profilers #1 and #2. These conclusions about
517 the locations of subsurface chlorophyll maxima are similar for both night and day occurrences (stars
518 and open circles in Figure 4, respectively), although SubMax_{>MLD} of day flagged profiles occurred
519 mostly at shallow depths (< 50 m, Figures 4b and 4d) and may result from an under-correction of the
520 surface quenched Chl-a concentrations (see Methods section 2.2). It seems that light limitation may
521 not be a major driver of subsurface Chl-a maxima via the mechanism of increased Chl-a production
522 per cell, at least under a certain threshold of Chl-a content, since SubMax_{>MLD} observed by bio-
523 profilers #3 and #4 occurred more frequently when the mixed layer was deep (for $2.5 \mu\text{g L}^{-1} \leq \text{Chl-a}$

524 $\leq 5 \mu\text{g L}^{-1}$; Figures 4c and 4f). However, the quasi-ubiquitous concomitance of SubMax_{>MLD} for bio-
525 profiler #1 with shallow mixed layers, less than 50 m, suggests that above a certain threshold of Chl-
526 a content, self-shading may promote pigment production by phytoplankton at depth.

527 Subsurface chlorophyll maxima beyond the reach of satellite imagery can be thought of as a
528 specific class of the wide range of possible chlorophyll distributions (such as varying thicknesses of
529 relatively constant near-surface biomass layers, or changes in the rate of decrease of biomass with
530 depth) that could introduce bias between surface concentration and water column inventory
531 perspectives. To gain perspective on the overall importance of these possibilities, we compared
532 surface chlorophyll concentrations measured by the profilers (using the shallowest ~10 m depth
533 observation since this was reliably within both the 1/e satellite ocean colour penetration depth and
534 the mixed layer) with their column inventories calculated from all observations in the top 200 m
535 (since chlorophyll distributions generally reduced to background values below this depth). These
536 comparisons, shown in Figure 5a (left column), display reasonably linear relationships over almost
537 the entire range of both night and daytime observations. This was especially true for bio-profilers #1
538 and #3 (correlation coefficients $r^2=[0.60-0.85]$), which include high chlorophyll values (greater than
539 2 mg m^{-3} for the surface concentration and greater than 160 mg m^{-2} for the 0-200 m inventory). Most
540 of the flagged daytime profiles (red circles in Figure 5a) seem to be shifted slightly left of the linear
541 regression lines, suggesting that they may well represent under-corrected quenched chlorophyll rather
542 than true features. Overall, qualitatively, these quite linear relationship between surface Chl-a
543 concentration and 0-200 m integrated Chl-a content suggests that satellite observations are reasonably
544 good indicators of the spatial distributions water column chlorophyll inventories.

545 Concerning the particulate backscattering signal, the linear correlations between surface values
546 and inventories were generally not as strong as for Chl-a, except for bio-profiler #3, as shown in
547 Figure 5b (right column: $r^2 = [0.29-0.74]$). It appears that surface b_{bp} values lower than $\sim 2 \times 10^{-3} \text{ m}^{-1}$
548 vary similarly to the 0-200 m b_{bp} inventories, whereas higher surface values exhibit noisier

549 correlations when compared to the 0-200 m integrated b_{bp} contents (see the slope breaks in the
550 relationship between surface and 0-200 m integrated b_{bp} in Figure 5b). The origin of this non-linearity
551 is not clear, and its evaluation is potentially compromised by the spikiness of the b_{bp} records and their
552 poor vertical resolution. The particulate backscatter profiles (Figures 2b, 3e and 9e) suggest that
553 spikes may be particularly common at the base of the mixed layer and below, and thus might reflect
554 differential control of phytoplankton and total particle populations. Future deployments with
555 improved firmware to yield higher resolution may be able to advance the interesting possibility that
556 backscatter information can provide ecosystem perspectives beyond phytoplankton biomass alone.

557 Because our qualitative assessment indicated that surface Chl-a concentrations provide a
558 relatively unbiased indication of the water column Chl-a inventory, we now try to go a little bit further
559 towards a quantitative assessment of possible biases between satellite and in-situ Chl-a perspectives.
560 First, we compared the coefficients of variation (i.e. the ratio of the standard deviation to the mean)
561 of the surface chlorophyll concentrations and of the water column inventories. Using only the night
562 data to avoid quenching correction uncertainties, surface distribution coefficients of variation (#1:
563 82%; #2: 20%; #3: 39%; #4: 43%) revealed very similar relative dispersions to the water column (0-
564 200 m) inventory coefficients of variation (#1: 84%; #2: 20%; #3: 34%; #4: 31%). Thus, satellite
565 images reasonably reflect the relative range of mesoscale variability in water column phytoplankton
566 biomass accumulations. Surprisingly, surface chlorophyll values (i.e. satellite images) would tend to
567 slightly overestimate the relative dispersion of Chl-a data for bio-profilers #3 and #4, despite those
568 profiles exhibiting the largest numbers of night subsurface maxima (in %, Table 3). This means that
569 the association of high surface chlorophyll concentrations with shallow chlorophyll layers was more
570 important than the presence of subsurface chlorophyll maxima in determining the relationships
571 between surface and water column inventories.

572 To further explore this issue, we calculated expected water column inventories for chlorophyll
573 layers confined to the physical mixed layer depths at the time of observation (by multiplying each
574 surface concentration by its associated mixed layer depth, MLD). This is akin to trying to improve

575 satellite assessments using mixed layer depth information from, for example, standard ARGO floats
576 that measure only temperature and salinity. These comparisons are shown in Figure 6a and reveal that
577 this approach badly underestimates water column inventories (at least with our MLD definition) and
578 that this underestimation is very common. Most of the “0-200 m integrated Chl-a/(surface Chl-a ×
579 MLD)” ratios range from 1/1 to 4/1, with a few profiles of bio-profilers #1 and #3, at the time when
580 they recorded the highest bio-optical values, reaching ratios of 20/1 (profiles ~ 70-130 for bio-profiler
581 #1 and profiles ~ 0-70 for bio-profiler #3). Moreover, the colour coding in Figure 6a shows that this
582 bias is strongest for shallow mixed layers in general. In other words, the presence of significant
583 amounts of chlorophyll below the mixed layer is very common (though generally not as local vertical
584 chlorophyll maxima, for which our statistics confine the occurrence of those exceeding 60% of
585 surface to 17% of the sampled locations and those exceeding 100% of surface to 11% of the sampled
586 locations). Notably, this bias still persists strongly if we change our MLD definition to the much
587 larger criterion of [Levitus \(1982\)](#); density increase of 0.125 kg m^{-3} relative to the density at 0 m). For
588 this criterion, the (surface Chl-a × MLD) estimation ranged between half and twice the 0-200 m
589 integrated Chl-a content for MLD deeper than 60 m (close to half for MLD ~ [60-90] m and surface
590 Chl-a $< 2 \mu\text{g L}^{-1}$ to close to twice for MLD > 120 m and surface Chl-a $> 2 \mu\text{g L}^{-1}$). However, (surface
591 Chl-a × MLD) estimations were still twice to four times lower than the 0-200 m integrated Chl-a
592 content recorded by the bio-profilers when the MLD ranges between 40 and 60 m (not shown).

593 The most probable explanation for these observations is that the mixed layer at the time of
594 observation was shallower than at the time of generation of the biomass. This is of course expected
595 as a result of seasonal shallowing of the mixed layer, but the magnitude of the effect is important to
596 recognize (as we have shown above) it is well above what could be corrected using some other mixed
597 layer depth criterion. Interestingly, there appears to be a relatively simple hyperbolic relationship
598 between the ratio “0-200 m integrated Chl-a” / “surface Chl-a × MLD” (hereafter designated as X)
599 and MLD, as shown in Figure 6b for the MLD definition of [Park et al. \(1998\)](#). It also holds for the

600 MLD definition of [Levitus \(1982\)](#). This X vs MLD hyperbola reaches an asymptote of $X \sim 1$ for MLD
601 values close to the 150-200 m depths of regional winter mixed layers (visible as temperature minima
602 remnant signatures of winter cooling in profiles south of the Polar Front in Figure 3b). Moreover, the
603 curve is reasonably well parameterized by $X \sim \text{MLD}^t / \text{MLD}^w$, in which the superscripts t and w
604 indicate mixed layer depths at the time of observation and the end of winter, respectively. This
605 relationship could arise if most biomass accumulation occurred in early deep mixed layers with
606 subsequent stratification adding little additional biomass, or if mixed layers shallowed and deepened
607 episodically as biomass accumulation developed throughout the season.

608 Overall, these results emphasize the major challenges that are present for connecting surface
609 chlorophyll distributions to total water column biomass and primary productivity, since they reveal
610 that physical mixed layer depths are often not a reliable guide to biomass distributions. These physical
611 and biological responses seem to be modulated differently on diel, weather, and seasonal timescales,
612 and are also affected by the mesoscale and sub-mesoscale interleaving of water parcels. The
613 quantification of near surface mixing (i.e. going beyond the limited mixed layer depth concept) is
614 currently under very active exploration and debate in the context of seasonal drivers of production
615 ([Behrenfeld, 2010](#); [Taylor and Ferrari, 2011](#)), and these data reveal the need to extend those
616 perspectives to shorter time and space scales. The presence of significant amounts of chlorophyll
617 below the mixed layer is also important to its ultimate fate –if this biomass is not re-entrained then it
618 may well contribute preferentially to export and to mesopelagic oxygen consumption (issues which
619 we revisit in Discussion section 4.3 below).

620 **4.2 Do regions of high biomass correlate with (local) oceanographic properties?**

621 To evaluate this issue, we examined bivariate regressions of Chl-a inventories (0-200 m) with
622 physical water column characteristics, after having separated the observations into two groups: 1)
623 Chl-a inventories $> 200 \text{ mg m}^{-2}$ in rich biomass regions close to the plateau, and 2) Chl-a inventories
624 $\leq 200 \text{ mg m}^{-2}$ in moderate biomass regions far from the plateau (the rich and moderate biomass

625 regions considered here are identified by red and yellow rectangles in Figures 3.1c, 3.2c, 3.3c and
626 3.4c). As shown in Figure 7 (a, b and c), the richest biomass regions encountered by bio-profiler #1
627 in 2011 and bio-profiler #3 in 2014 were associated with waters with very similar properties,
628 specifically moderate temperatures (3.5-5 °C), high salinities (33.82-33.85), and thus relatively high
629 densities (sigma-theta values of 26.7-26.9 kg m⁻³). The bio-profiler #1 distributions of chlorophyll
630 with these properties showed linear decreases on either side of these values, suggestive of mixing
631 with surrounding waters much poorer in Chl-a. This characteristic is also observed between integrated
632 Chl-a and mean surface oxygen saturation (O_{2 sat}, Figure 7f), for which the high O_{2 sat} states (reaching
633 10%) indicate oxygen production in these high biomass waters (since these values exceeding expected
634 from processes such as warming or bubble injection; [Shadwick et al., 2014](#)). Relatively high biomass
635 was also encountered in waters with extreme T-S properties (the warmest and freshest observed) in
636 the vicinity of the Gallieni Spur by bio-profiler #4 (black symbols in Figure 7). Thus, there was not a
637 unique class of waters with high biomass. This perspective is further reinforced by the lack of any
638 clear relationships between chlorophyll inventories and local water column properties for regions of
639 moderate biomass, including versus mixed layer depth and the intensity of stratification as
640 represented by the Brunt-Väisälä frequency (Figure 7, right column). These low biomass waters also
641 exhibited lower O_{2 sat} states (95-103%) than those of rich biomass areas. The under-saturated oxygen
642 levels reflect either strong local respiration or the supply of low oxygen waters from below, with
643 these processes difficult to distinguish (except for specific portions of the bio-profiler #4 trajectory
644 where time series within constant physical property layers were obtained, as discussed in section 4.3).

645 Linking local water parcel properties to past water trajectories with respect to the Kerguelen
646 Plateau, as a known natural source of iron fertilization, provides an additional view of the role of
647 water mass properties in the control of chlorophyll inventories. For the richest Chl-a waters (T ~ 4
648 °C, S ~ 33.83, σ ~ 26.8 kg m⁻³) encountered by bio-profiler#1, surface drifters released during the
649 KEOPS2 voyage ([d'Ovidio et al., 2014](#)) suggest these waters derive from the northern Kerguelen

650 plateau. The computation of trajectories based on satellite altimetry (see Methods section 2.3) for all
651 the bio-profilers confirms this perspective and also indicates that the time since a water mass left the
652 plateau (Figure 8b) is another important determinant of chlorophyll levels (presumably as a result
653 loss of Fe over time after its addition from the plateau; [d'Ovidio et al., 2014](#)). These results are shown
654 in Figure 8. Figure 8 b) and d) compares water age and origin with the 0-200 m Chl-a inventories for
655 spring (bio-profiler #1, in blue in the plots) and summer (bio-profilers #2, #3, #4, in black in the
656 plots). Beside a strong seasonal difference –spring values range from up to 1000 mg m⁻², whereas in
657 the summer few measurements exceed 300 mg m⁻²– water parcels corresponding to high Chl-a
658 inventories appear to be waters that have recently left the Kerguelen Plateau (20-40 days of water
659 age; Figure 8a) and come generally from its northern part ([-49; -47] °S; Figure 8c). Bio-profilers
660 locations that correspond to water parcels that have not touched the Plateau in the last 100 days (points
661 shown in white for water age = 100 in Figure 8b) do not present any high integrated Chl-a values,
662 suggesting that the main source of iron fertilization for the explored water masses is horizontal
663 advection from the Kerguelen Plateau. This correlation of high Chl-a inventories with age since
664 leaving the plateau is unlikely to be biased by the lower frequency of sampling (shown in the Figure
665 8b inset) of older waters, given that a statistical test based a 10⁴ samplings of a uniform distribution
666 of integrated Chl-a at the sampling frequency of each water age yielded a probability (p) of not-
667 sampling integrated Chl-a value greater than 200 mg m⁻² for water parcels with water ages greater
668 than 40 days of $p < 10^{-4}$.

669 These results suggest that the northern Kerguelen Plateau is an important target region for future
670 studies of iron delivery mechanisms into the plume downstream. In terms of the secondary influences
671 of mixed layer depth and stratification, the bio-profiler #1 profiles with integrated Chl-a greater than
672 600 mg m⁻² were mainly characterized by a shallow mixed layer, lower than 60 m (Figure 7d), and a
673 low stratification ($-0.01 \text{ s}^{-2} < \max N^2 < 0 \text{ s}^{-2}$; Figure 7e). Below this Chl-a inventory threshold, no
674 clear relationships emerged between MLD or N^2 and 0-200 m integrated chlorophyll (Figures 7d and
675 7e). In a steady state perspective, this lack of correlation could arise because mixed layers were

676 shallow enough that light limitation was not sufficient to halt phytoplankton accumulation, yet not so
677 shallow that mean mixed layer light levels allowed light promoted growth to reach accumulations
678 that became self-shading (viewpoints that have been developed previously, based on relationships
679 between fluorescence and mixed layer depth observations in this region using sensors on elephant
680 seals; [Blain et al., 2013](#)). Importantly, our observations emphasize that chlorophyll distributions do
681 not track the shoaling of mixed layer depth on seasonal or weather timescales, and thus that MLD
682 variability is unlikely to show simple relationships to biomass accumulation. This point has also been
683 emphasized in terms of competing effects of light and Fe limitation responses to MLD variability
684 ([Joubert et al., 2014](#)), for waters where vertical Fe supply is dominant (rather than the horizontal
685 dominance of supply studied here).

686

687 **4.3 Can the fate of surface enrichments in biomass be determined, and if so, what is the** 688 **percentage of biological production exported?**

689 Evaluating this question requires the extraction of a temporal perspective from the bio-profiler
690 records, and is thus only possible for portions of their trajectories which appear to be essentially
691 Lagrangian. The best record for this approach is for bio-profiler #4 during the period when it carried
692 out several clockwise loops in late autumn, i.e. for profiles 150-240 (Figure 3.4a). During this time,
693 its trajectory was very similar to that expected based on surface currents estimated from satellite
694 altimetry, the density stratification of the water column was relatively steady, and the T-S profiles
695 were tightly grouped (Figures 9b, 9c and 9d). These observations suggest that the profiler remained
696 within a single water parcel, that was entrained by a retentive eddy and underwent only small
697 exchanges with surrounding waters, as shown by slightly warmer (profiles 165-170 and 200-220) and
698 cooler (profiles 175-195) conditions along the trajectory (these are discussed further below).

699 At the start of this period (blue lines subset in Figure 9e), chlorophyll profiles showed moderate
700 to high surface and subsurface layer levels, well above HNLC background values, with some profiles
701 exhibiting subsurface maxima reaching up to $1.5 \mu\text{g L}^{-1}$ between 50-70 m depth and up to $1 \mu\text{g L}^{-1}$
702 around 120 m depth. Both the surface constant Chl-a layer and the subsurface “chlorocline” layer (by
703 analogy to thermocline or halocline, “chlorocline” is defined here as the depth range with the highest
704 chlorophyll concentration gradient) were thick, equal to ~ 80 m and ~ 50 m, respectively. The origin
705 of the smaller and variable subsurface maxima seen in some profiles in Figure 9e is uncertain. One
706 possibility is that they are remnants of the high surface chlorophyll biomass observed just prior to the
707 eddy entrainment (visible in Figure 3.4c and the “bloom 2013” animation in the supplementary
708 material), that had been carried to depth by particle settling or by subduction of the denser, saltier,
709 and slightly cooler water associated with that high biomass. Associated b_{bp} profiles showed similar
710 large variations with strong local maxima correlated to local Chl-a maxima (blue lines subset in
711 Figure 9f). The strong variability of the Chl-a/ b_{bp} profiles over the first 100 m suggests possible
712 changes in the composition of the particulate assemblage (blue lines subset in Figure 9g).

713 During the Lagrangian eddy entrainment period, the surface mixed layer chlorophyll levels
714 declined further from $1.5 \mu\text{g L}^{-1}$ to $\sim 1 \mu\text{g L}^{-1}$ (Figure 3.4c and 9e). Since the constant chlorophyll
715 surface layer shallowed progressively with time, this Chl-a decrease did not result from the possible
716 effect of dilution by mixed layer deepening (i.e. entrainment). Furthermore, the chlorocline content
717 decreased briefly before re-increasing progressively in its upper part, and then its deeper part. In
718 parallel, b_{bp} and Chl-a/ b_{bp} profiles became tighter and tighter (light blue to orange profiles in Figures
719 9f and 9g) before re-exhibiting larger variations (red profiles). These results suggest the possibility
720 of some chlorophyll conversion to non-fluorescent material, or its removal by export to depth or by
721 local respiration or both, throughout the eddy entrainment. They may also of course partly reflect
722 small spatial variations in the structure of the biomass distributions.

723 To evaluate these possibilities we examined changes in three layers, the surface layer (labelled
724 layer 1 and defined as the surface down to the 26.6 isopycnal surface), and two density layers

725 immediately below it (layers 2 and 3, respectively for density ranges 26.6-26.8 and 26.8-26.9). In
726 order to characterize the existence of vertical or horizontal mixing during the eddy entrainment, mean
727 temperature, salinity, depth of the density layers, as well as their thickness and their stratification
728 state, are shown in Figure 10 (a, b, and c). The thickness and mean depth of the surface density layer
729 were relatively constant in the first half of the eddy entrainment, then slightly increased as some
730 warmer and fresher - thus lighter - water entered into the eddy structure (profiles 200-220).
731 Contrastingly, the physical properties of the two deeper underlying density layers showed
732 insignificant temporal trends and smaller variability over the period of interest, and thus changes in
733 their biogeochemical properties can be attributed to local processes rather than exchanges.

734 The evolution of chlorophyll, particulate backscattering and dissolved oxygen inventories also
735 exhibited different trends and variability for each layer (as shown in Figure 10d, e and f). In surface
736 layer 1, mean chlorophyll and b_{bp} showed no overall temporal trend (green and grey curves in Figure
737 10d, respectively), although characterized by two maxima, one at the beginning of the eddy and one
738 coinciding with the fresher warmer water occurrence described above. The oxygen content
739 continuously decreased steadily until after profile 200, when larger variations were observed, with a
740 minimum content coinciding with the fresher warmer waters. Within the underlying layer 2,
741 chlorophyll, b_{bp} and oxygen inventories showed similar evolutions: all had maximums at the
742 beginning of the eddy and then decreased with time until the bio-profiler exited the eddy (Figure 10e).
743 These characteristics were also present in the deepest layer 3, although with significant differences in
744 the magnitudes of change, specifically the oxygen decrease was similar to that of layer 2, but the
745 chlorophyll level and its absolute magnitude of decrease were much smaller, and the b_{bp} levels
746 remained relatively high for a longer portion of the record.

747 To verify that these changes were oceanographic, we again evaluated fluorometer and oxygen
748 sensor drifts, but this time only over the range of profiles considered for the eddy entrainment
749 investigation (following the approach used in Table 2, of examining the evolution of the mean values

750 within the depth layer 950-1000 m). Chl-a and O₂ drifts were respectively estimated to be +0.017 μg
751 L⁻¹ and +1.05 μmol kg⁻¹. Thus, the temporal drifts probably lead to underestimations of the observed
752 decrease of Chl-a (of ~7% in layer 2 and of ~20% in layer 3) and of O₂ (~30% in layers 2 and 3).
753 Knowing that excluding the contribution of the drifts would only reinforce the trends described above,
754 we can now suggest the following overall interpretation to explain these variations of Chl-a, b_{bp} and
755 O₂ in these 3 density layers during the eddy entrainment of bio-profiler #4. In the surface layer 1, the
756 chlorophyll inventory seems to result from the combination of local biological processes with weak
757 horizontal resupply from warmer, fresher, and less oxygenated water (Figures 9a and 9d). In the
758 middle density layer 2, where mixing is considered insignificant because of the tightly grouped T-S
759 properties, the chlorophyll decrease does not seem to be due to local transformation to non-fluorescent
760 detritus since no corresponding increase in the b_{bp} signal was observed (Figure 10e). This leaves loss
761 by settling or respiration as possible explanations. Loss by settling is certainly possible on this
762 timeframe (rates of only a few meters per day are required), and the high b_{bp} values found in the lower
763 density layer 3 around profiles 160-180 could reflect transfer from the overlying layer 2. Biomass
764 loss by respiration and remineralization to dissolved inorganic carbon is almost certainly also
765 occurring given the decreasing oxygen inventories of the middle layer 2 and deep layer 3. For both
766 these layers the rate of chlorophyll loss is too small (by factors of 2-3, assuming a moderately high
767 phytoplankton C/Chl-a ratio of 50) to explain all the oxygen decrease, implying that degradation of
768 detritus (represented by the decreasing particulate backscattering signal) and dissolved organic matter
769 probably also contributes (this remains true even if we use a very high phytoplankton C/Chl-a ratio
770 of 100; [Cloern et al., 1995](#)). For the deepest layer 3, remineralization of settling particles coming from
771 above with a minor remineralization of local chlorophyll may best explain the slower decrease of
772 chlorophyll in comparison to that of oxygen.

773 In combination, these results suggest that not all of the accumulated biomass was respired in the
774 surface layer, with the CO₂ then returned to the atmosphere, and thus that there was some export.
775 Quantifying this export amount is difficult and merits a modelling and sensitivity assessment that is

776 beyond the scope of this paper. Here we simply provide an indication of its possible magnitude by
777 comparison of the rates of mean oxygen loss in the surface layer 1 (representing carbon likely to be
778 returned to the atmosphere) versus the subsurface layers 2 and 3 (representing carbon which may be
779 exported in the ocean interior). The linear fits to the oxygen decreases for layers 1, 2, and 3 (as shown
780 in Figure 10) imply oxygen consumption rates of approximately 5, 4, and 4 $\mu\text{mol m}^{-3} \text{d}^{-1}$, respectively.
781 These values lie towards the lower end of estimates for annual rates at mesopelagic depths ([Sarmiento
782 et al., 1990](#)). Comparing O_2 consumption of layers 2 and 3 (by multiplying the O_2 consumption rate
783 by the thickness and the average density of the layer) relative to the total mean consumption among
784 the three layers, we estimate that 35% of the CO_2 produced during this autumn period of bloom
785 decline was exported from the surface layer (with 20% respired within layer 2 and 15% within layer
786 3). An analogous area of low-to-moderate production and relatively high export was observed during
787 the KEOPS2 field cruise just south of Polar Front, in a meander area around $72.5^\circ \text{E} - 49^\circ \text{S}$ where
788 the flow – considered as Lagrangian – was sampled in few stations as a time series ([Laurenceau-
789 Cornec et al., 2015](#); [Planchon et al., 2014](#)). This area coincides with the location of the anti-cyclonic
790 trajectory of bio-profiler #3, around profile #110, where moderate biomass production was observed
791 (Figure 3.3c), although spatial variations in this region unfortunately precluded estimation of
792 biologically driven oxygen consumption from the bio-profiler.

793

794 **5 Conclusions**

795 The bio-profilers revealed several interesting aspects of the enriched biomass plume downstream
796 from the Kerguelen plateau, by providing observations of its vertical dimension. First of all, the
797 observations show that surface and total water column chlorophyll inventories are generally well
798 correlated, which suggests that satellite perspectives on bloom spatial dynamics (e.g. [Mongin et al.,
799 2008](#); [2009](#)) are unlikely to be strongly biased. This result holds true despite the presence of moderate

800 (60% above surface values) subsurface chlorophyll maxima in up to ~20% of all the profiles, and
801 strong (100% above surface values) in ~10% of all the profiles (Table 3 and Figure 4). Furthermore,
802 satellite surface observations seem to well reflect the water column relative range of mesoscale
803 variability in biomass accumulations. However, the retrieval of water column Chl-a inventory from
804 satellite surface observations is not simple. The bio-profilers often recorded significant quantities of
805 biomass below the diel mixed layer, potentially correlated to the degree of shallowing of the mixed
806 layer from deep winter values. The mixed layer at the time of the observations may not be the best
807 parameter to quantify the chlorophyll inventories, especially when stratification by advection of
808 lighter water mass or by seasonal warming creates strong density variations in the upper layer and,
809 thus, shallow mixed layers, and considering that chlorophyll production may have occurred much
810 earlier than at the time of the observations. And of course, our work does not imply that satellite
811 chlorophyll estimates are necessarily accurate. That is an issue which our data cannot address owing
812 to the imprecision of the bio-optical sensors and the absence of calibration against local chlorophyll
813 observations, an approach which recent work has shown to be necessary for satellite estimates as well
814 ([Johnson et al., 2013](#)).

815 The occurrence of moderate subsurface chlorophyll maxima in our data (17%) was higher than
816 for results obtained with fluorescence sensors deployed on elephant seals around the Kerguelen
817 plateau (~9% using a criterion of 30% excess over surface values to define the maxima; [Guinet et al.,](#)
818 [2012](#)). This may reflect the greater proportion of observations in the southern portion of the plume in
819 the [Guinet et al. \(2012\)](#) study, a region where we also found that subsurface maxima were less
820 common (~4% of profiles for bio-profiler #2 for our moderate criterion of 60% excess, Table 3, and
821 ~6% using their 30% criterion, data not shown). Subsurface maxima were also uncommon well
822 downstream to the east of the Kerguelen plateau. This is interesting in that it suggests that subsurface
823 iron levels supplied by upwelling or vertical mixing were insufficient to drive biomass accumulations
824 at the base of the mixed layer, or at least were less important than horizontal supply of Fe in surface
825 waters. This is in contrast to Polar Frontal Zone waters much further to the east south of Australia

826 where persistent subsurface maxima have been observed ([Parslow et al., 2001](#)), and with observations
827 from other autonomous profiling floats elsewhere in the Southern Ocean in which small subsurface
828 maxima were found to be common in summer below the mixed layer ([Carranza et al., 2014](#)).
829 Variations in the relative intensities of surface and deep iron supplies is a possible cause of these
830 variations, but other processes may also be involved. As an example, the origin of the relatively more
831 common and stronger subsurface chlorophyll maxima near the Gallieni Spur is not clear. Settling of
832 surface biomass generated earlier in the season (Figure 1) and/or seasonal depletion of iron in surface
833 waters which reduces phytoplankton growth rates are possibilities, but they cannot be assessed given
834 our lack of early seasonal observations. A third possibility of the overlaying of low density waters
835 southward across the Polar Front appears less likely, given that shipboard observations during
836 KEOPS2 found that this process generated shallow high biomass layers (at the Polar Frontal stations
837 F-L, TEW-7, and TEW-8; ([Lasbleiz et al., 2014](#); [Trull et al., 2015](#)).

838 Our initial research goals included looking for oxygen supersaturations in deep chlorophyll
839 maxima to estimate net community production ([Spitzer and Jenkins, 1989](#)), but this could not be
840 achieved owing to confounding effects on super-saturations from strong mixing with higher
841 productivity overlying waters, and on aliasing of daily cycles by internal waves ([Park et al., 2008a](#)).
842 Thus our results cannot address the issues of whether productivity in subsurface layers may partly
843 explain offsets between satellite and in-situ estimates of the Southern Ocean biological pump
844 ([Schlitzer, 2002](#)) or whether the phytoplankton that grow in deep chlorophyll maxima are preferential
845 contributors to carbon export ([Kemp et al., 2000](#); [Queguiner, 2013](#)). We were able to make a first
846 simple assessment of subsurface autumn oxygen consumption during the portion of the bio-profiler
847 #4 trajectory that delivered a quasi-Lagrangian time series, and this provided the very useful result
848 that approximately 35% of the biomass respiration in that period occurred beneath the mixed layer,
849 and thus at depths favouring CO₂ export toward the ocean interior. This 35% can be approximately
850 equated to an export/production “e-ratio” of 0.4, which is relatively high by global standards, but in

851 the middle of the large range of values observed in cold Southern Ocean waters ([Maiti et al., 2013](#)),
852 and similar to f-ratios estimated for high biomass waters over the central Kerguelen plateau in autumn
853 during the KEOPS1 campaign ([Trull et al., 2008](#)). Of course the subsequent fate of the exported CO₂
854 inferred from the bio-profiler #4 observations is uncertain, in that these waters were still within the
855 depth range of possible exposure to the atmosphere during later deeper winter mixing, although the
856 larger scale circulation in this region suggests it is a region dominated by subduction ([Sallée et al.,
857 2010](#)).

858 Our simple correlative evaluation of the bio-profiler observations of biomass variations
859 revealed that the highest chlorophyll levels were observed in surface waters with a narrow range of
860 densities and moderate temperatures ($\sigma\sim 26.9 \pm 0.05 \text{ kg m}^{-3}$, $T \sim 4 \pm 0.5^\circ\text{C}$; Figure 7). This occurrence of
861 maximum biomass at moderate temperatures, along with the lack of correlation with mixed layer
862 depth (Figure 7) suggests that local controls on growth rates were less important than the history of
863 the levels of iron supplied in this water type. Notably, water with these properties was found
864 preferentially near the northern Kerguelen plateau and Gallieni Spur suggesting iron supply from this
865 region. This is consistent with geostrophic circulation estimates and a favourable wind regime for
866 upwelling in this region during the 2011 KEOPS2 period when bio-profiler #1 was deployed
867 ([d'Ovidio et al., 2014](#); [Gille et al., 2014](#)) and with Lagrangian analyses that backtrack water parcels
868 to identify their origin. Further observations and analyses are of course necessary to determine the
869 generality of this inference that the northern Kerguelen plateau provides the major source of iron to
870 the downstream biomass plume. This is especially true given the limited seasonal and inter-annual
871 scope of our bio-profiler observations.

872

873 *Acknowledgements*

874 This work was supported by the Australian Commonwealth Cooperative Research Program via the
875 ACE CRC. M. Grenier was supported by a conjoint LEGOS and ACE CRC postdoctoral appointment

876 and a CAMPUS FRANCE grant (FASIC award # 30418QG; campusfrance.org). A. Della Penna was
877 supported by a conjoint Frontières du Vivant (Paris 7) and CSIRO-UTAS Quantitative Marine
878 Science PhD scholarship. We thank Ann Thresher (CSIRO) for the harvesting and processing of the
879 data from the bio-profilers, as supported by the Australian Integrated Marine Observing Argo and
880 Southern Ocean Time Series facilities. We thank Cedric Cotté and Francesco d'Ovidio (LOCEAN,
881 Université de Paris VI) and the crew of the *RV Marion Dufresne* for bio-profiler deployments, and
882 Stephane Blain and Bernard Quéguiner for KEOPS2 voyage leadership. Thanks to Vito Dirita, Alan
883 Poole, and Craig Hanstein (CSIRO) for bio-profiler preparation, and Craig Neill and Kelly Brown
884 (CSIRO) for oxygen optode calibrations. Thanks to Helen Phillips (IMAS) for fruitful discussions
885 and advice concerning physical analyses of the hydrological variables, and Francesco d'Ovidio
886 (LOCEAN, CNRS) for insights into Lagrangian perspectives on water parcel trajectories and their
887 evolution. Finally, we gratefully acknowledge Dr S. Thomalla and an anonymous reviewer for their
888 valuable comments on an earlier version of the paper that allowed us to improve it significantly.

889

890 **List of Tables**

891 Table 1. Bio-profiler deployments.

892 Table 2. Drift assessment of the bio-profilers over their life time within the [250-300] m and [950-
893 1000] m depth layers.

894 Table 3. Fluorescence quenching corrections and subsurface chlorophyll maxima statistics.

895 **Figure Captions**

896 Figure 1. Maps of bio-profiler trajectories (white and grey lines) over remotely sensed chlorophyll-a
897 distributions (a-h: daily, 4 km CLS/CNES product; i: weekly composite from GlobColour 4 km
898 product). Top row: 2011 bloom season for bio-profiler #1. Middle and bottom rows: 2013/2014
899 bloom and beginning of post-bloom season for bio-profilers #2 (light grey trajectory), #3 (dark grey
900 trajectory) and #4 (white trajectory). Red squares indicate the bio-profiler locations corresponding
901 to the day of the image. The black thick line refers to the position of the Polar Front measured from
902 hydrographic samples by [Park et al. \(2014a\)](#).

903

904 Figure 2. a) Assessment of bio-optical sensor stability from temporal evolution of chlorophyll and
905 particulate backscattering values averaged over two depth ranges, 250-300 m (lines) and 950-1000
906 m (stars). Arrows indicate profiles considered to be affected by bio-fouling, which were not used in
907 further analysis. b) Illustration of quenching corrections, showing pairs of successive night/day
908 profiles (day: continuous lines; night: dashed lines). For each bio-profiler, the panel shows:
909 chlorophyll profiles without quenching correction (left), chlorophyll profiles with quenching
910 correction (middle), and associated particulate backscattering profiles (right). Squares in the middle
911 panel represent threshold values of the lowest surface chlorophyll concentration for the night
912 profiles of each bio-profiler (#1: $0.7 \mu\text{g L}^{-1}$; #2: $0.4 \mu\text{g L}^{-1}$; #3: $0.65 \mu\text{g L}^{-1}$; #4: $0.7 \mu\text{g L}^{-1}$). These
913 threshold were used to flag day profiles having surface chlorophyll concentration still below this
914 threshold after the quenching correction (see Table 3, Figures 4 (squares), 5 (red circles) and 7
915 (squares)), for which quenching might have been under-corrected. c) Comparison of bio-profiler #1
916 fluorescence Chl-a estimates to shipboard results obtained by the KEOPS2 project: c.i. Location of
917 KEOPS2 stations E1 (blue symbols) and E2 (black symbols) along a quasi-Lagrangian track
918 followed by bio-profiler#1 (red symbols); c.ii Temperature profiles showing similar structures of
919 the ship and bio-profiler sampled water columns; c.iii Fluorescence profiles (lines) showing that the

920 bio-profiler provided similar fluorescence results to the ship CTD mounted sensor, and that both
921 exhibited complex relationships to Niskin bottle total chlorophyll-a sample values (dots; see text for
922 further discussion).

923

924 Figure 3.1. Bio-profiler #1 observations

925 a) bio-profiler #1 trajectory over the bathymetry, with each point representing a depth profile and
926 the colour of the points changing from blue to red over time (dates are shown below the bottom
927 plots). The 700 m isobath is represented by the red line contour. KI = Kerguelen Island; KP =
928 Kerguelen Plateau; HI = Heard Island; GS = Gallieni Spur. b-f) Evolution of hydrological
929 parameters along the float trajectory: b) temperature ($^{\circ}\text{C}$), c) chlorophyll ($\mu\text{g L}^{-1}$), d) salinity
930 (unitless), e) particulate backscattering (b_{bp} ; log scale; m^{-1}), and f) dissolved oxygen ($\mu\text{mol kg}^{-1}$).
931 The white line represents the mixed layer depth. Red and yellow rectangles refer to rich and
932 moderate chlorophyll areas used in Figure 7 and discussed in Section 4.2.

933

934 Figure 3.2. Bio-profiler #2 observations (see Figure 3.1 caption for details).

935

936 Figure 3.3. Bio-profiler #3 observations (see Figure 3.1 caption for details).

937

938 Figure 3.4. Bio-profiler #4 observations (see Figure 3.1 caption for details).

939

940 Figure 4. Characteristics of subsurface chlorophyll maxima occurring at depths greater than the
941 mixed layer depth and exceeding the surface content by more than 60% (top) and 100% (bottom). a)
942 and d): geographical areas where these subsurface Chl-a maxima occur with an expanded view for

943 the Gallieni Spur region; b) and e): associated depths of these subsurface Chl-a maxima along the
944 bio-profiler trajectories (i.e. versus profile numbers); c) and f): relationship between the amplitude
945 of these Chl-a maxima (in $\mu\text{g L}^{-1}$) and the mixed layer depth (MLD, in m). Symbols: stars refer to
946 night profiles, circles to day profiles and squares to flagged day profiles (i.e. which still exhibit, in
947 the surface layer, a large concentration decrease toward low surface values that indicates the
948 possibility of incomplete quenching correction; see definition in the caption of Figure 2b).

949

950 Figure 5. a) Surface chlorophyll concentrations (in mg m^{-3}) compared to chlorophyll inventories (0-
951 200 m; in mg m^{-2}), for each bio-profiler. b) Surface particulate backscattering (m^{-1}) compared to
952 particulate backscattering inventories (0-200 m), for each bio-profiler. Note that scales are slightly
953 larger for bio-profiler #1 than for the others; the dashed rectangles in upper plots indicate the scales
954 used for the other bio-profilers. Night profiles (black circles), day profiles (green circles) and
955 potentially quenching under-corrected day profiles (red circles, flagged as defined in the caption of
956 Figure 2b) are distinguished. Correspondingly, the green and black lines refer to the linear
957 regression of day and night profiles, and their associated correlation coefficients, r^2 .

958

959 Figure 6: a) Chlorophyll water column inventories (in mg m^{-2}), estimated by multiplying surface
960 chlorophyll concentrations by the mixed layer depth, compared to chlorophyll inventories (0-200 m;
961 in mg m^{-2}) recorded by the bio-profilers. Only night and unflagged day profiles are represented. The
962 colour code shows the associated depth of the mixed layer (in m). The 5 lines $y = x$, $y = 2x$, $y = 4x$,
963 $y = 8x$ and $y = 20x$ are given as indicators to quantify the ratio between the “surface Chl-a \times MLD”
964 product and the 0-200 m integrated Chl-a.

965 b) Representation of the X factor ($X = (0\text{-}200 \text{ m integrated Chl-a}) / (\text{surface Chl-a} \times \text{MLD})$) as a

966 function of the mixed layer depth (in m), for the total data set. Symbols and colours are defined in
967 the legend.

968

969 Figure 7. Relationship between 0-200 m integrated chlorophyll a concentration and various water
970 properties for a-f) high biomass regions close to the plateau (bio-profilers #1 and #3) or entrapped
971 in eddies (bio-profilers #2 and #4; red rectangles in Figures 3.1, 3.2, 3.3 and 3.4) and g-l) moderate
972 biomass regions far from the plateau (yellow rectangles in Figures 3.1, 3.2, 3.3 and 3.4). a) and g):
973 surface temperature (in °C); b) and h): surface salinity (unitless); c) and i): surface density (in kg m⁻³);
974 d) and j) mixed layer depth (MLD; in m); e) and k) maximum Brunt-Väisälä frequency squared
975 (N^2 ; in s⁻²) f) and l) oxygen saturation state (in %). Symbols and colours are defined in the legend.

976

977 Figure 8: Lagrangian diagnostics computed from altimetry. Maps of age and origins of the water
978 parcels shown in plots (a) and (c) are from Figure 4 of d'Ovidio et al. (2014). White pixels represent
979 water parcels that have not touched in the past 100 days the Kerguelen Plateau (defined by the 700
980 m isobath and shown in grey). Comparison of these age and origin metrics with the bio-profiler
981 total integrated Chlorophyll-a values are shown in plots (b) and (d). Blue dots correspond to data
982 collected during spring (bio-profiler #1, mean values in red) and black dots to data collected during
983 summer (bio-profilers #2, #3, #4, mean values in magenta). White dots correspond to water parcels
984 that have not touched the Kerguelen Plateau. The inset in plot b) shows the number of
985 measurements for each water age. The black arrow highlights the fact that low Chl-a levels
986 associated with water parcels that have not touched the Kerguelen Plateau within the last 100 days
987 is supported by a large number of samples and, thus, seems to be a robust feature.

988

989 Figure 9. Eddy entrapment of bio-profiler #4.

- 990 a) Identification of entrainment along the bio-profiler trajectory, with the colour of the points
991 changing, from blue to red over time, from profile 150 to profile 240.
- 992 b) Overlay of bio-profiler trajectory (white line) and eddy retention indices, showing the portion of
993 the trajectory within a long-lasting (more than 30 days) retentive structure. The red square marks
994 the temporal reference (profile 177) from which the Lagrangian trajectories were computed for the
995 retention statistic, as described in Methods section 2.3.
- 996 c) Temperature-salinity diagram. Colours correspond to location on the map in a).
- 997 d) Temperature versus depth section with mixed layer depth (black line) and isopycnals indicated
998 (white lines).
- 999 e) Chlorophyll profiles, coloured as on the map and separated, for the sake of clarity, in 4 subsets of
1000 ~23 profiles (equivalent to ~2 weeks of data acquisition).
- 1001 f) As e), but for particulate backscattering (b_{bp}) profiles.
- 1002 g) As e), but for the chlorophyll/ b_{bp} ratio.

1003 Note that chlorophyll and b_{bp} signals were filtered for visual clarity, using a 3 point running median.

1004

1005 Figure 10: Temporal evolution of physical and biological properties during the eddy entrainment of
1006 bio-profiler #4 for three density layers: with sigma-theta ranges of surface-26.6; 26.6-26.8; 26.8-
1007 26.9. Left column plots a-c) show physical properties: mean depth (in m; black line and scale),
1008 thickness (in m, dashed black line and black scale), temperature (θ , in $^{\circ}\text{C}$; red line and scale),
1009 salinity (S, unitless; blue line and scale), density (σ , in kg m^{-3} ; purple line and scale) and Brunt-
1010 Väisälä frequency squared (N^2 , in s^{-2} ; gray line and scale). Right column plots d-f) show
1011 biogeochemical properties: mean chlorophyll (Chl-a, in $\mu\text{g L}^{-1}$; green line and scale), particulate

1012 backscattering (b_{bp} , in m^{-1} ; gray line and scale), and oxygen concentrations (O_2 , in $\mu mol\ kg^{-1}$;
1013 orange line and scale).

1014 **References**

- 1015 Assmy, P., Smetacek, V., Montresor, M., Klaas, C., Henjes, J., Strass, V. H., Arrieta, J. M.,
1016 Bathmann, U., Berg, G. M., and Breitbarth, E.: Thick-shelled, grazer-protected diatoms decouple
1017 ocean carbon and silicon cycles in the iron-limited Antarctic Circumpolar Current, *Proceedings*
1018 *of the National Academy of Sciences*, 110, 20633-20638, 2013.
- 1019
- 1020 Babin, M., Morel, A., and Gentili, B.: Remote sensing of sea surface sun-induced chlorophyll
1021 fluorescence: consequences of natural variations in the optical characteristics of phytoplankton
1022 and the quantum yield of chlorophyll a fluorescence, *International Journal of Remote Sensing*,
1023 17(12), 2417-2448, 1996.
- 1024
- 1025 Behrenfeld, M. J.: Abandoning Sverdrup's Critical Depth Hypothesis on phytoplankton blooms,
1026 *Ecology*, 91(4), 977-989, 2010.
- 1027
- 1028 Biermann, L., Guinet, C., Bester, M., Brierley, A., and Boehme1, L.: An alternative method for
1029 correcting fluorescence quenching, *Ocean Science*, 11, 83–91, 2015.
- 1030
- 1031 Blain, S., Queguiner, B., Armand, L., Belviso, S., Bombled, B., Bopp, L., Bowie, A., Brunet, C.,
1032 Brussaard, C., Carlotti, F., Christaki, U., Corbiere, A., Durand, I., Ebersbach, F., Fuda, J.-L.,
1033 Garcia, N., Gerringa, L., Griffiths, B., Guigue, C., Guillerm, C., Jacquet, S., Jeandel, C., Laan,
1034 P., Lefevre, D., Lo Monaco, C., Malits, A., Mosseri, J., Obernosterer, I., Park, Y.-H., Picheral,
1035 M., Pondaven, P., Remenyi, T., Sandroni, V., Sarthou, G., Savoye, N., Scouarnec, L., Souhaut,
1036 M., Thuiller, D., Timmermans, K., Trull, T., Uitz, J., van Beek, P., Veldhuis, M., Vincent, D.,
1037 Viollier, E., Vong, L., and Wagener, T.: Effect of natural iron fertilization on carbon
1038 sequestration in the Southern Ocean, *Nature*, 446, 1070-U1071, 10.1038/nature05700, 2007.
- 1039
- 1040 Blain, S., Queguiner, B., and Trull, T.: The natural iron fertilization experiment KEOPS (KErguelen
1041 Ocean and Plateau compared Study): An overview, *Deep-Sea Research Part II-Topical Studies in*
1042 *Oceanography*, 55, 559-565, 10.1016/j.dsr2.2008.01.002, 2008.
- 1043
- 1044 Blain, S., Renaut, S., Xing, X., Claustre, H., and Guinet, C.: Instrumented elephant seals reveal the
1045 seasonality in chlorophyll and light-mixing regime in the iron-fertilized Southern Ocean,
1046 *Geophysical Research Letters*, 40, 1-5, doi:10.1002/2013GL058065,052013, 2013.
- 1047
- 1048 Blain, S., Capparos, J., Guéneuguès, A., Obernosterer, I., and Oriol, L.: Distributions and
1049 stoichiometry of dissolved nitrogen and phosphorus in the iron-fertilized region near Kerguelen
1050 (Southern Ocean), *Biogeosciences*, 12, 623–635, 2015.
- 1051
- 1052 Boss E., and Pegau, W. S.: Relationship of light scattering at an angle in the backward direction to
1053 the backscattering coefficient, *Applied Optics*, 40(30), 5503–5507, 2001.
- 1054

- 1055 Boyd, P., LaRoche, J., Gall, M., Frew, R., and McKay, R. L. M.: Role of iron, light, and silicate in
1056 controlling algal biomass in subantarctic waters SE of New Zealand, *Journal of Geophysical*
1057 *Research*, 104, 13395-13408, 1999.
- 1058
- 1059 Boyd, P. W., Crossley, A. C., DiTullio, G. R., Griffiths, F. B., Hutchins, D. A., Queguiner, B.,
1060 Sedwick, P. N., and Trull, T. W.: Control of phytoplankton growth by iron supply and irradiance
1061 in the subantarctic Southern Ocean: Experimental results from the SAZ Project, *Journal of*
1062 *Geophysical Research*, 106, 31573-31584, 2001.
- 1063
- 1064 Boyd, P. W., Jickells, T., Law, C. S., Blain, S., Boyle, E. A., Buesseler, K. O., Coale, K. H., Cullen,
1065 J. J., Baar, H. J. W. d., Follows, M., Harvey, M., Lancelot, C., Levasseur, M., Owens, N. P. J.,
1066 Pollard, R., Rivkin, R. B., Sarmiento, J., Schoemann, V., Smetacek, V., Takeda, S., Tsuda, A.,
1067 Turner, S., and Watson, A. J.: Mesoscale Iron Enrichment Experiments 1993-2005: Synthesis
1068 and Future Directions, *Science*, 315, 612 - 617, DOI: 610.1126/science.1131669, 2007.
- 1069
- 1070 Boyd, P. W., and Trull, T. W.: Understanding the export of marine biogenic particles: is there
1071 consensus?, *Progress in Oceanography*, 4, 276-312, doi:210.1016/j.pocean.2006.1010.1007,
1072 2007.
- 1073
- 1074 Boyd, P. W., and Ellwood, M. J.: The biogeochemical cycle of iron in the ocean, *Nature*
1075 *Geoscience*, 3, 675 - 682, 10.1038/ngeo964, 2010.
- 1076
- 1077 Carranza, M. M., Gille, S. T., Franks, P. J. S., Girton, J. B., and Johnson, K. S.: Mixed-layer depth
1078 and Chl-a variability in the Southern Ocean, *ICES Journal of Marine Science*, submitted, 2014.
- 1079
- 1080 Cavagna, A. J., Fripiat, F., Elskens, M., Dehairs, F., Mangion, P., Chirurgien, L., Closset,
1081 I., Lasbleiz, M., Flores-Leiva, L., Cardinal, D., Leblanc, K., Fernandez, C., Lefèvre, D., Oriol,
1082 L., Blain, S., and Quéguiner, B.: Biological productivity regime and associated N cycling in the
1083 vicinity of Kerguelen Island area, Southern Ocean, *Biogeosciences Discuss.*, 11, 18073-18104,
1084 2014.
- 1085
- 1086 Cetinić, I., Perry, M. J., Briggs, N. T., Kallin, E., D'Asaro, E. A., and Lee, C. M.: Particulate
1087 organic carbon and inherent optical properties during 2008 North Atlantic Bloom Experiment,
1088 *Journal of Geophysical Research*, 117, C06028, doi:10.1029/2011JC007771, 2012.
- 1089
- 1090 Cloern, J. E., Grenz, C., and Videgar-Lucas, L.: An empirical model of the phytoplankton
1091 chlorophyll: carbon ratio-the conservation factor between productivity and growth rate,
1092 *Limnology and Oceanography*, 40, 1313-1321, 1995.
- 1093
- 1094 Constable, A. J., Nicol, S., and Strutton, P. G.: Southern Ocean productivity in relation to spatial
1095 and temporal variation in the physical environment, *Journal of Geophysical Research - Oceans*,
1096 108, 8079, doi:8010.1029/2001JC001270, 2003.

1097

1098 Cullen, J. J.: The deep chlorophyll maximum: comparing vertical profiles of chlorophyll a,
1099 *Canadian Journal of Fisheries and Aquatic Sciences*, 39(5), 791-803, 1982.

1100

1101 d'Ovidio, F., Della Penna, A., Trull, T., Nencioli, F., Pujol, I., Rio, M.H., Park, Y.H., Cott ,C.,
1102 Zhou, M. and Blain, S. , The biogeochemical structuring role of horizontal stirring: Lagrangian
1103 perspectives on iron delivery downstream of the Kerguelen plateau, *Biogeosciences Discussions*,
1104 2014.

1105

1106 d'Ovidio, F., De Monte, S., Della Penna, A., Cotté, C., and Guinet, C.: Ecological implications of
1107 eddy retention in the open ocean: a Lagrangian approach, *Journal of Physics A: Mathematical
1108 and Theoretical*, 46, 254023, 2013.

1109

1110 de Baar, H. J. W., de Jong, J. T. M., Bakker, D. C. E., Loscher, B. M., Veth, C., Bathmann, U., and
1111 Smetacek, V.: Importance of iron for phytoplankton blooms and carbon dioxide drawdown in the
1112 Southern Ocean, *Nature*, 373, 412-415, 1995.

1113

1114 Earp, A., Hanson, C. E., Ralph, P. J., Brando, V. E., Allen, S., Baird, M., Clementson, L., Daniel,
1115 P., Dekker, A. G., and Fearn, P. R.: Review of fluorescent standards for calibration of in situ
1116 fluorometers: Recommendations applied in coastal and ocean observing programs, *Optics
1117 express*, 19, 26768-26782, 2011.

1118

1119 Falkowski, P. G., and Kiefer, D. A.: Chlorophyll a fluorescence in phytoplankton: relationship to
1120 photosynthesis and biomass, *Journal of Plankton Research*, 7(5), 715-731, 1985.

1121

1122 Falkowski, P. G., and Kolber, Z.: Variations in chlorophyll fluorescence yields in phytoplankton in
1123 the world oceans, *Australian Journal of Plant Physiology*, 22, 341–355, 1995.

1124

1125 Fennel, K., and Boss, E.: Subsurface maxima of phytoplankton and chlorophyll: Steady - state
1126 solutions from a simple model, *Limnology and Oceanography*, 48(4), 1521-1534, 2003.

1127

1128 Gille, S. T., Carranza, M. M., Cambra, R., and Morrow, R.: Wind-induced upwelling in the
1129 Kerguelen Plateau Region, *Biogeosciences*, 11, 6389–6400, 2014.

1130

1131 Goericke, R., and Montoya, J. P.: Estimating the contribution of microalgal taxa to chlorophyll a in
1132 the field-variations of pigment ratios under nutrient-and light-limited growth, *Marine Ecology
1133 Progress Series*, 169, 97-112, 1998.

1134

- 1135 Gordon, H. R., and McCluney, W. R.: Estimation of the depth of Sun light penetration in the sea for
1136 remote sensing, *Appl. Opt.*, 14, 413-416, 1975.
- 1137
- 1138 Guinet, C., Xing, X., Walker, E., Monestiez, P., Marchand, S., Picard, B., Jaud, T., Authier, M.,
1139 Cotté, C., and Dragon, A.-C.: Calibration procedures and first data set of Southern Ocean
1140 chlorophyll a profiles collected by elephant seal equipped with a newly developed CTD-
1141 fluorescence tags, *Earth System Science Data Discussions*, 5, 853-891, 2012.
- 1142
- 1143 Huot, Y., Babin, M., Bruyant, F., Grob, C., Twardowski, M. S., and Claustre, H.: Relationship
1144 between photosynthetic parameters and different proxies of phytoplankton biomass in the
1145 subtropical ocean, *Biogeosciences*, 4, 853–868, 2007.
- 1146
- 1147 Johnson, R., Strutton, P. G., Wright, S. W., McMinn, A., and Meiners, K. M.: Three improved
1148 satellite chlorophyll algorithms for the Southern Ocean, *Journal of Geophysical Research-*
1149 *Oceans*, 118, 1-10, 2013.
- 1150
- 1151 Jouandet, M.-P., Trull, T. W., Guidi, L., Picheral, M., Ebersbach, F., Stemmann, L., and Blain, S.:
1152 Optical imaging of mesopelagic particles indicates deep carbon flux beneath a natural iron-
1153 fertilized bloom in the Southern Ocean, *Limnology and Oceanography*, 56(3), 1130-1140,
1154 doi:10.4319/lo.2011.56.3.1130., 2011.
- 1155
- 1156 Joubert, W., Swart, S., Tagliabue, A., Thomalla, S., and Monteiro, P.: The sensitivity of primary
1157 productivity to intra-seasonal mixed layer variability in the sub-Antarctic Zone of the Atlantic
1158 Ocean, *Biogeosciences Discussions*, 11(3), 4335-4358, 2014.
- 1159
- 1160 Kemp, A. E. S., Pike, J., Pearce, R. B., and Lange, C. B.: The 'Fall dump' - a new perspective on the
1161 role of a 'shade flora' in the annual cycle of diatom production and export flux, *Deep Sea*
1162 *Research II*, 47, 2129-2154, 2000.
- 1163
- 1164 Kiefer, D. A.: Fluorescence properties of natural phytoplankton populations, *Marine Biology*, 22,
1165 263–269, 1973.
- 1166
- 1167 Lasbleiz, M., Leblanc, K., Blain, S., Ras, J., Cornet-Barthaux, V., Hélias Nunige, S., and
1168 Quéguiner, B.: Pigments, elemental composition (C, N, P, Si) and stoichiometry of particulate
1169 matter, in the naturally iron fertilized region of Kerguelen in the Southern Ocean,
1170 *Biogeosciences*, 11, 5931–5955, 2014.
- 1171
- 1172 Laurenceau-Cornec, E. C., Trull, T. W., Davies, D. M., Bray, S. G., Doran, J., Planchon, F.,
1173 Carlotti, F., Jouandet, M. P., Cavagna, A. J., Waite, A. M., and Blain, S.: The relative importance
1174 of phytoplankton aggregates and zooplankton fecal pellets to carbon export: insights from free-
1175 drifting sediment trap deployments in naturally iron-fertilised waters near the Kerguelen plateau,
1176 *Biogeosciences*, 12, 1007–1027, 2015.

1177

1178 Le Quéré, C., Takahashi, T., Buitenhuis, E. T., Rödenbeck, C., and Sutherland, S. C.: Impact of
1179 climate change and variability on the global oceanic sink of CO₂, *Global Biogeochemical*
1180 *Cycles*, 24(GB4007), doi:10.1029/2009GB003599, 2010.

1181

1182 Lenton, A., Tilbrook, B., Law, R. M., Bakker, D., Doney, S. C., Gruber, N., Ishii, M., Hoppema,
1183 M., Lovenduski, N. S., Matear, R. J., McNeil, B. I., Metzl, N., Mikaloff Fletcher, S. E.,
1184 Monteiro, P. M. S., Rödenbeck, C., Sweeney, C., and Takahashi, T.: Sea-air CO₂ fluxes in the
1185 Southern Ocean for the period 1990–2009, *Biogeosciences*, 10, 4037–4054; doi:210.5194/bgd-
1186 5110-5285-5201, 2013.

1187

1188 Levitus, S.: Climatological atlas of the world ocean, NOAA Prof. Pap. 13, 173 pp., U.S. Govt.
1189 Printing Off., Washington, D. C., 1982.

1190

1191 Levy, M.: Mesoscale variability of phytoplankton and of new production: Impact of the large-scale
1192 nutrient distribution, *Journal of Geophysical Research*, 108(C11), 3358,
1193 doi:3310.1029/2002JC001577, 2003.

1194

1195 Maiti, K., Charette, M. A., Buesseler, K. O., and Kahru, M.: An inverse relationship between
1196 production and export efficiency in the Southern Ocean, *Geophysical Research Letters*, 40,
1197 1557-1561, 2013.

1198

1199 Martin, J. H.: Glacial-interglacial CO₂ change: The iron hypothesis, *Paleoceanography*, 5, 1-13,
1200 1990.

1201

1202 Martinez, E., Antoine, D., D’Ortenzio, F., and Gentili, B.: Climate-driven basin-scale decadal
1203 oscillations of oceanic phytoplankton, *Science*, 326, 1253-1256, 2009.

1204

1205 Matear, R., Hirst, A. C., and McNeil, B. I.: Changes in dissolved oxygen in the Southern Ocean
1206 with climate change, *Geochemistry, Geophysics, Geosystems*, 1(www.g-cubed.org), paper
1207 #2000GC000086, 2000.

1208

1209 Mongin, M., Molina, E., and Trull, T. W.: Seasonality and scale of the Kerguelen plateau
1210 phytoplankton bloom: A remote sensing and modeling analysis of the influence of natural iron
1211 fertilization in the Southern Ocean, *Deep-Sea Research II*, 55, 880-892,
1212 10.1016/j.dsr2.2007.12.039, 2008.

1213

- 1214 Mongin, M., Abraham, E. R., and Trull, T. W.: Winter advection of iron can explain the summer
1215 phytoplankton bloom that extends 1000 km downstream of the Kerguelen Plateau in the
1216 Southern Ocean, *Journal of Marine Research*, 67, 225-237, 2009.
- 1217
- 1218 Moore, J. K., and Abbott, M. R.: Phytoplankton chlorophyll distributions and primary production in
1219 the Southern Ocean, *Journal of Geophysical Research*, 105(C12), 28,709–728,722, 2000.
- 1220
- 1221 Morel, A., and Maritorena, S.: Bio-optical properties of oceanic waters: A reappraisal, *Journal of*
1222 *Geophysical Research*, 106 (C4), 7163-7180, 2001.
- 1223
- 1224 Mosseri, J., Queguiner, B., Armand, L.K., and Cornet-Barthaux V.: Impact of iron on silicon
1225 utilization by diatoms in the Southern Ocean: A case study of Si/N cycle decoupling in a
1226 naturally iron-enriched area. *Deep-Sea Research II*, 55: 801-819, 2008.
- 1227
- 1228 Nicol, S., Pauly, T., Vindoff, N., Wright, S., Thiele, D., Hosie, G., Strutton, P., and Woehler, E.:
1229 Ocean circulation off East Antarctica affects ecosystem structure and sea-ice extent, *Nature*, 406,
1230 504-507, 2000.
- 1231
- 1232 Nielsdóttir, M. C., Bibby, T. S., Moore, C. M., Hinz, D. J., Sanders, R., Whitehouse, M. J., Korb, R.
1233 E., and Achterberg, E. P.: Seasonal and spatial dynamics of iron availability in the Scotia Sea,
1234 *Marine Chemistry*, 130-131, 62-72, 2012.
- 1235
- 1236 Oka, E., and Ando, K.: Stability of temperature and conductivity sensors of Argo profiling floats,
1237 *Journal of oceanography*, 60, 253-258, 2004.
- 1238
- 1239 Orsi, A. H., Whitworth, T. I., and Nowlin, W. D. J.: On the meridional extent and fronts of the
1240 Antarctic Circumpolar Current, *Deep-Sea Research*, 42, 641-673, 1995.
- 1241
- 1242 Park, Y.-H., Fuda, J.-L., Durand, I., and Naveira Garabato, A. C.: Internal tides and vertical mixing
1243 over the Kerguelen Plateau, *Deep Sea Research Part II: Topical Studies in Oceanography*, 55,
1244 582-593, 2008a.
- 1245
- 1246 Park, Y.-H., Roquet, F., Fuda, J.-L., and Durand, I.: Large scale circulation over and around the
1247 Kerguelen Plateau, *Deep Sea Research II*, 55, 566-581, 2008b.
- 1248
- 1249 Park, Y.-H., Charriaud, E., Ruiz Pino, D., and Jeandel, C.: Seasonal and interannual variability of
1250 the mixed layer properties and steric height at station KERFIX, southwest of Kerguelen, *Journal*
1251 *of Marine Systems*, 17, 571–586, 1998.
- 1252
- 1253 Park, Y.-H., Durand, I., Kestenare, E., Rougier, G., Zhou, M., d'Ovidio, F., Cotté, C., and Lee, J.-
1254 H.: Polar Front around the Kerguelen Islands: An up-to-date determination and associated

- 1255 circulation of surface/subsurface waters, *Journal of Geophysical Research Oceans*, 119, 6575–
1256 6592, doi:10.1002/2014JC010061, 2014a.
- 1257
- 1258 Park, Y.-H., Lee, J.-H., Durand, I., and Hong, C.-S.: Validation of the Thorpe scale-derived vertical
1259 diffusivities against microstructure measurements in the Kerguelen region, *Biogeosciences*, 11,
1260 6927-6937, 2014b.
- 1261
- 1262 Parslow, J., Boyd, P., Rintoul, S. R., and Griffiths, F. B.: A persistent sub-surface chlorophyll
1263 maximum in the Polar Frontal Zone south of Australia: seasonal progression and implications for
1264 phytoplankton-light-nutrient interactions, *Journal of Geophysical Research*, 106, 31543-31557,
1265 2001.
- 1266
- 1267 Planchon, F., Ballas, D., Cavagna, A.-J., Bowie, A., Davies, D., Trull, T., Laurenceau, E., van der
1268 Merwe, P., and Dehairs, F.: Carbon export in the naturally iron-fertilized Kerguelen area of the
1269 Southern Ocean based on the ²³⁴Th approach, *Biogeosciences Discuss.*, 11, submitted, 2014.
- 1270
- 1271 Pollard, R. T., I.Salter, Sanders, R. J., Lucas, M. I., Moore, C. M., Mills, R. A., Statham, P. J.,
1272 Allen, J. T., Baker, A. R., Bakker, D. C. E., Charette, M. A., Fielding, S., Fones, G. R., French,
1273 M., Hickman, A. E., Holland, R. J., Hughes, J. A., Jickells, T. D., Lampitt, R. S., Morris, P. J.,
1274 Nédélec, F. H., Nielsdóttir, M., Planquette, H., Popova, E. E., Poulton, A. J., Read, J. F.,
1275 Seeyave, S., Smith, T., Stinchcombe, M., Taylor, S., Thomalla, S., Venables, H. J., Williamson,
1276 R., and Zubkov, M. V.: Southern Ocean deep-water carbon export enhanced by natural iron
1277 fertilization, *Nature*, 457, 577-580, doi:510.1038/nature07716, 2009.
- 1278
- 1279 Queguiner, B.: Iron fertilization and the structure of planktonic communities in high nutrient
1280 regions of the Southern Ocean, *Deep Sea Research II*, 90, 43-54, 2013.
- 1281
- 1282 Sackmann, B. S., Perry, M. J., and Eriksen, C. C.: Seaglider observations of variability in daytime
1283 fluorescence quenching of chlorophyll-a in Northeastern Pacific coastal waters, *Biogeosciences*
1284 *Discussions*, 5, 2839–2865, 2008.
- 1285
- 1286 Sallée, J.-B., Speer, K., Rintoul, S., and Wijffels, S.: Southern Ocean thermocline ventilation,
1287 *Journal of Physical Oceanography*, 40, 509-529, 2010.
- 1288
- 1289 Salter, I., Lampitt, R. S., Sanders, R., Poulton, A., Kemp, A. E. S., Boorman, B., Saw, K., and
1290 Pearce, R.: Estimating carbon, silica and diatom export from a naturally fertilised phytoplankton
1291 bloom in the Southern Ocean using PELAGRA: A novel drifting sediment trap, *Deep Sea*
1292 *Research II*, 54, 2233-2259, 2007.
- 1293

- 1294 Sanial, V., van Beek, P., Lansard, B., d'Ovidio, F., Kestenare, E., Souhaut, M., Zhou, M., and Blain,
1295 S.: Study of the phytoplankton plume dynamics off the Crozet Islands (Southern Ocean): A
1296 geochemical- physical coupled approach, *Journal of Geophysical Research: Oceans*, 119.4
1297 2227-2237, 2014.
- 1298
- 1299 Sarmiento, J. L., Thiele, G., Key, R. M., and Moore, W. S.: Oxygen and nitrate new production and
1300 remineralization i the North Atlantic subtropical gyre, *Journal of Geophysical Research: Oceans*,
1301 95, 18303-18315, 1990.
- 1302
- 1303 Sarmiento, J. L., and Le Quéré, C.: Oceanic carbon dioxide uptake in a model of century-scale
1304 global warming, *Science*, 274, 1346-1350, 1996.
- 1305
- 1306 Sarmiento, J. L., Gruber, N., Brzezinski, M. A., and Dunne, J. P.: High-latitude controls of
1307 thermocline nutrients and low latitude biological productivity, *Nature*, 427, 56-60, 2004.
- 1308
- 1309 Savoye, N., Dehairs, F., Elskens, M., Cardinal, D., Kopczynska, E. E., Trull, T. W., Wright, S.,
1310 Baeyens, W., and Griffiths, F. B.: Regional variation of spring N-uptake and new production in
1311 the Southern Ocean, *Geophysical Research Letters*, 31, L03301,
1312 doi:03310.01029/02003GL018946, 2004.
- 1313
- 1314 Savoye, N., Trull, T. W., Jacquet, S. H. M., Navez, J., and Dehairs, F.: ²³⁴Th-based export fluxes
1315 during a natural iron fertilization experiment in the Southern Ocean (KEOPS), *Deep Sea*
1316 *Research II*, 55(5-7), 841-855, 2008.
- 1317
- 1318 Schlitzer, R.: Carbon export fluxes in the Southern Ocean: results from inverse modeling and
1319 comparison with satellite-based estimates, *Deep-Sea Research II*, 49, 1623-1644, 2002.
- 1320
- 1321 Shadwick, E. H., Tilbrook, B., Cassar, N., Trull, T. W., and Rintoul, S. R.: Summertime physical
1322 and biological controls on O₂ and CO₂ in the Australian Sector of the Southern Ocean, *Journal of*
1323 *Marine System*, doi: 10.1016/j.jmarsys.2013.12.008, 2014.
- 1324
- 1325 Shadwick, E. H., Trull, T. W., Tilbrook, B., Sutton, A., Schulz, E., and Sabine, C. L.: Seasonality of
1326 biological and physical controls on surface ocean CO₂ from hourly observations at the Southern
1327 Ocean Time Series site south of Australia, *Global Biogeochemical Cycles*, 29, 223–238, doi:
1328 10.1002/2014GB004906, 2015.
- 1329
- 1330 Sigman, D. M., and Boyle, E. A.: Glacial/Interglacial variations in atmospheric carbon dioxide,
1331 *Nature*, 407, 859-869, 2000.
- 1332

- 1333 Sokolov, S., and Rintoul, S. R.: Circumpolar structure and distribution of the Antarctic Circumpolar
1334 Current fronts: 1. Mean circumpolar paths, *Journal of geophysical research*, 114, C11018, 2009.
- 1335
- 1336 Sokolov, S., and Rintoul, S. R.: On the relationship between fronts of the Antarctic Circumpolar
1337 Current and surface chlorophyll concentrations in the Southern Ocean, *J. Geophys. Res. –*
1338 *Oceans*, 112(C07030), doi: 10.1029/2006JC004072, 2007.
- 1339
- 1340 Spitzer, W. S., and Jenkins, W. J.: Rates of vertical mixing, gas exchange and new production:
1341 Estimates from seasonal gas cycles in the upper ocean near Bermuda, *Journal of Marine*
1342 *Research*, 47, 169-196, 1989.
- 1343
- 1344 Stramski, D., Reynolds, R. A., Babin, M., Kaczmarek, S., Lewis, M. R., Röttgers, R., Sciandra, A.,
1345 Stramska, M., Twardowski, M. S., Franz, B. A., and Claustre, H.: Relationships between the
1346 surface concentration of particulate organic carbon and optical properties in the eastern South
1347 Pacific and eastern Atlantic Oceans, *Biogeosciences*, 5, 171–201, 2008.
- 1348
- 1349 Suggett, D. J., Prášil, O., and Borowitzka, M. A.: *Chlorophyll a fluorescence in aquatic sciences:*
1350 *methods and applications*, Springer, 2011.
- 1351
- 1352 Sullivan, J. M., Twardowski, M. S., Zaneveld, R. J. V., and Moore, C. C.: Measuring optical
1353 backscattering in water, in *Light Scattering Reviews 7: Radiative Transfer and Optical Properties*
1354 *of Atmosphere and Underlying Surface*, A. Kokhanovsky, ed. (Springer Praxis Books, 2013), pp.
1355 189–224.
- 1356
- 1357 Sverdrup, H. U.: On the conditions for the vernal blooming of phytoplankton, *Journal du Conseil*
1358 *Internationale Permanente pour l'Exploration de la Mer*, 18, 287-295, 1953.
- 1359
- 1360 Swart, S., Thomalla, S., and Monteiro, P.: The seasonal cycle of mixed layer dynamics and
1361 phytoplankton biomass in the Sub-Antarctic Zone: A high-resolution glider experiment, *Journal*
1362 *of Marine Systems*, 2014.
- 1363
- 1364 Taylor, J. R., and Ferrari, R.: Shutdown of turbulent convection as a new criterion for the onset of
1365 spring phytoplankton blooms, *Limnology and Oceanography*, 56(6), 2293–2307, 2011.
- 1366
- 1367 Thomalla, S. J., Fauchereau, N., Swart, S., and Monteiro, P. M. S.: Regional scale characteristics of
1368 the seasonal cycle of chlorophyll in the Southern Ocean, *Biogeosciences*, 8(10), 2849-2866,
1369 doi:10.5194/bg-8-2849-2011, 2011.
- 1370

- 1371 Trull, T. W., Davies, D., and Casciotti, K.: Insights into nutrient assimilation and export in naturally
1372 iron-fertilized waters of the Southern Ocean from nitrogen, carbon and oxygen isotopes, *Deep-*
1373 *Sea Research Part Ii-Topical Studies in Oceanography*, 55, 820-840, 10.1016/j.dsr2.2007.12.035,
1374 2008.
- 1375
- 1376 Trull, T. W., Davies, D. M., Dehairs, F., Cavagna, A. J., Lasbleiz, M., Laurenceau, E. C., d'Ovidio,
1377 F., Planchon, F., Leblanc, K., Quéguiner, B., and Blain, S.: Chemometric perspectives on
1378 plankton community responses to natural iron fertilization over and downstream of the
1379 Kerguelen Plateau in the Southern Ocean, *Biogeosciences*, 12, 1029–1056, 2015.
- 1380
- 1381 Trull, T. W., Bray, S. G., Manganini, S. J., Honjo, S., and François, R.: Moored sediment trap
1382 measurements of carbon export in the Subantarctic and Polar Frontal Zones of the Southern
1383 Ocean, south of Australia, *Journal of Geophysical Research*, 106, 31489-31510, 2001.
- 1384
- 1385 Watson, A. J., Bakker, D. C. E., Ridgwell, A. J., Boyd, P. W., and Law, C. S.: Effect of iron supply
1386 on Southern Ocean CO₂ uptake and implications for glacial for atmospheric CO₂, *Nature*, 407,
1387 730-733, 2000.
- 1388
- 1389 Weeding, B., and Trull, T. W.: Hourly oxygen and total gas tension measurements at the Southern
1390 Ocean Time Series site reveal winter ventilation and spring net community production, *Journal*
1391 *of Geophysical Research - Oceans*, 119, 348-358, doi:310.1002/2013JC009302, 002014, 2014.
- 1392
- 1393 Xing, X., Claustre, H., Blain, S., d'Ortenzio, F., Antoine, D., Ras, J., and Guinet, C.: Quenching
1394 correction for in vivo chlorophyll fluorescence acquired by autonomous platforms: A case study
1395 with instrumented elephant seals in the Kerguelen region (Southern Ocean), *Limnology and*
1396 *Oceanography: Methods*, 10, 483–495, 2012.
- 1397
- 1398 Zhang, X., Hu, L., and He, M.-X.: Scattering by pure seawater: effect of salinity, *Opt.Express*, 17,
1399 5698–5710, 2009.
- 1400

1401 Table 1. Bio-profiler deployments

1402

1403

#	Hull#*	WMO#**	UTC Date	Lat. (° N)	Long. (° E)	Campaign	Last profile (UTC Date)	
1404	1	5122	1901329	29 Oct 2011	-48.5	72.2	KEOPS2	22 Apr 2012
1405	2	6684	5904882	26 Jan 2014	-49.9	76.2	MYCTO	14 Apr 2014
1406	3	6682	1901338	28 Jan 2014	-48.4	71.5	MYCTO	14 Apr 2014
1407	4	6683	1901339	4 Feb 2014	-48.6	74.0	MYCTO	14 Apr 2014

1408

1409 * Hull#: serial number for the bio-profiler body

1410 ** WMO#: World Meteorological Organization identification number for the bio-profiler data stream

1411 Table 2. Drift assessment of the bio-profilers over their life time within the [250-300] m and [950-
1412 1000] m depth layers

1413

1414 ***Chlorophyll concentration drift within the [250-300] m depth layer***

#	Mean slope ($\mu\text{g L}^{-1} \text{ profile}^{-1}$)	Mean absolute drift ^a ($\mu\text{g L}^{-1}$)	Mean drift relative to the mean surface Chl-a concentration ^b
1 ^c	8.4050 E-5	0.0252	+1 %
2	-1.7832 E-4	-0.0531	-5 %
3	-2.8722 E-4	-0.0798	-6 %
4	-1.1976 E-4	-0.0304	-3 %

1421

1422 ***Chlorophyll concentration drift within the [950-1000] m depth layer***

#	Mean slope ($\mu\text{g L}^{-1} \text{ profile}^{-1}$)	Mean absolute drift ^a ($\mu\text{g L}^{-1}$)	Mean drift relative to the mean surface Chl-a concentration ^b
1	-	-	-
2	-2.1917 E-6	-0.0007	< -1 %
3	-9.0120 E-5	-0.0251	-2 %
4	1.2438 E-5	0.0032	< +1 %

1429

1430 ***Particulate backscattering drift within the [250-300] m depth layer***

#	Mean slope (m^{-1})	Mean absolute drift ^a (m^{-1})	Mean drift relative to the mean surface b_{bp} ^d
1 ^c	1.1625 E-6	3.4876 E-04	+11 %
2	-1.1613 E-6	-3.4608 E-04	-19 %
3	-1.9682 E-7	-5.4716 E-05	-2 %
4	-6.7301 E-7	-1.7094 E-04	-10 %

1437

1438 ***Particulate backscattering drift within the [950-1000] m depth layer***

#	Mean slope (m^{-1})	Mean absolute drift ^a (m^{-1})	Mean drift relative to the mean surface b_{bp} ^d
1	-	-	-
2	-2.2931 E-7	-6.8335 E-05	-4 %
3	-4.4734 E-7	-1.2436 E-04	-6 %
4	-2.0227 E-7	-5.1378 E-05	-3 %

1445

1446 ^a= mean slope * nb of profiles

1447 ^b= mean slope * nb of profiles / mean chlorophyll concentration

1448 ^c Calculated between profiles #1 and profile #300, and excluding the deep biomass production
1449 profiles (range #[100-171])

1450 ^d= mean slope * nb of profiles / mean particulate backscattering

1451 Table 3. Fluorescence quenching corrections and subsurface chlorophyll maxima statistics

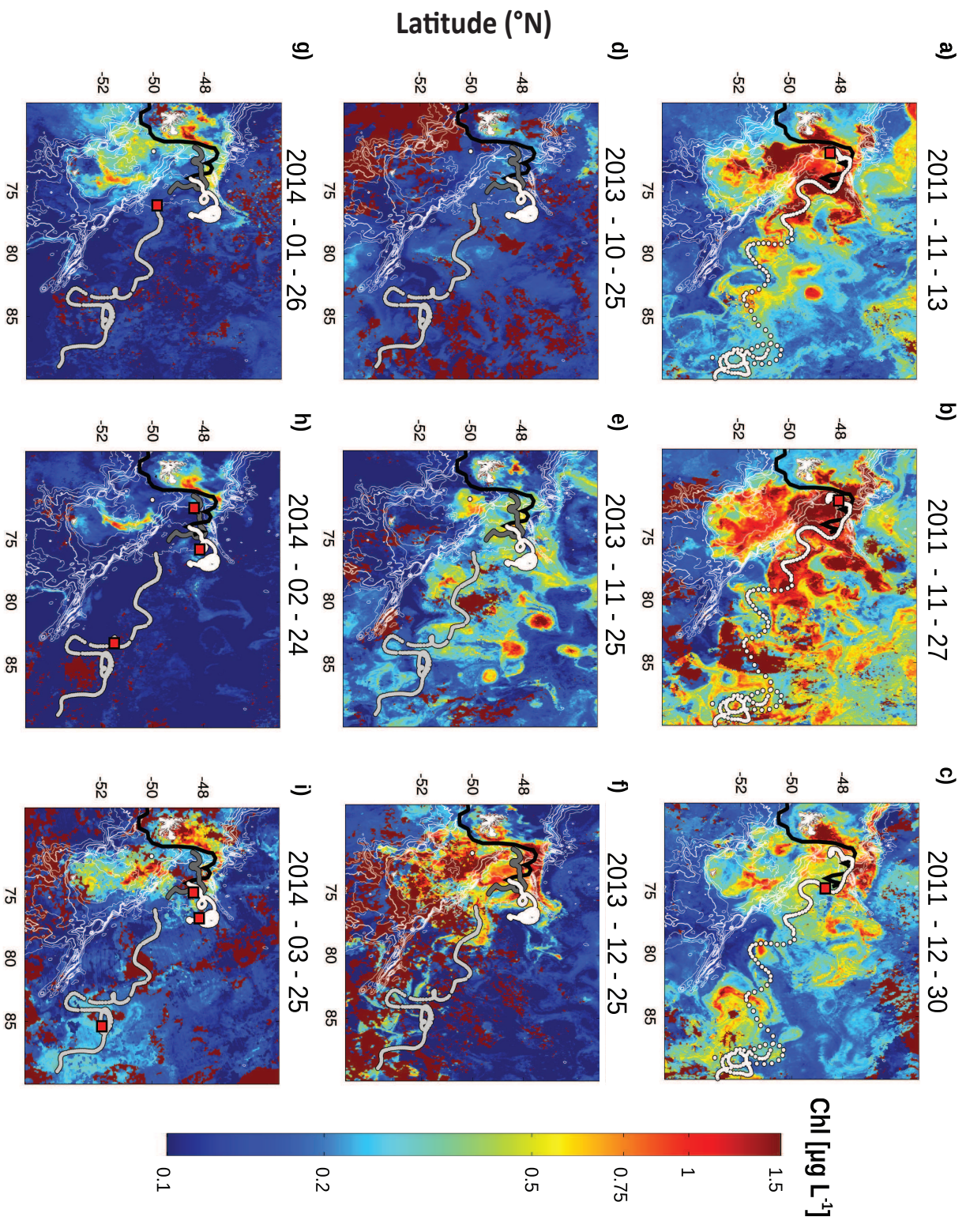
1452

Individual bio-profiler statistics	#1	#2	#3	#4
Fluorescence profiles collected	384	298	278	254
Fluorescence profiles usable	300	298	277	254
Night time profiles	129	143	133	119
Day time profiles	171	155	144	135
Night time profiles with subsurface maxima ^a total /within the ML/below the ML (% of night time profiles)	17/5/12/ (13/4/9)%	3/1/2 (2/1/1)%	24/9/15 (18/7/11)%	25/14/11 (21/12/9)%
Day time profiles with subsurface maxima ^a before correction total /within the ML/below the ML (% of daytime profiles)	142/62/80 (83/36/47)%	93/55/38 (60/35/25)%	105/48/57 (73/33/40)%	95/40/55 (70/30/40)%
Quenching corrected profiles (and among them, number of corrected profiles which still exhibit low surface values ^c)	170 (22)	155 (6)	139 (12)	127 (18)
Day time profiles with subsurface maxima ^a after correction total /within the ML/below the ML (% of corrected day profiles)	40/0/40 (24/0/24)%	10/1/9 (6/0/6)%	32/3/29 (23/2/21)%	40/9/31 (31/7/24)%
Total night and corrected day profiles with moderate subsurface maxima ^a total /within the ML/below the ML (% of night and corrected day profiles)	57/5/52 (19/2/17)%	13/2/11 (4/1/3)%	56/12/44 (20/4/16)%	65/23/42 (26/9/17)%
Total night and corrected day profiles with large subsurface maxima ^b total /within the ML/below the ML (% of night and corrected day profiles)	32/1/31 (10/0/10)%	6/0/6 (2/0/2)%	36/5/31 (13/2/11)%	45/15/30 (18/6/12)%

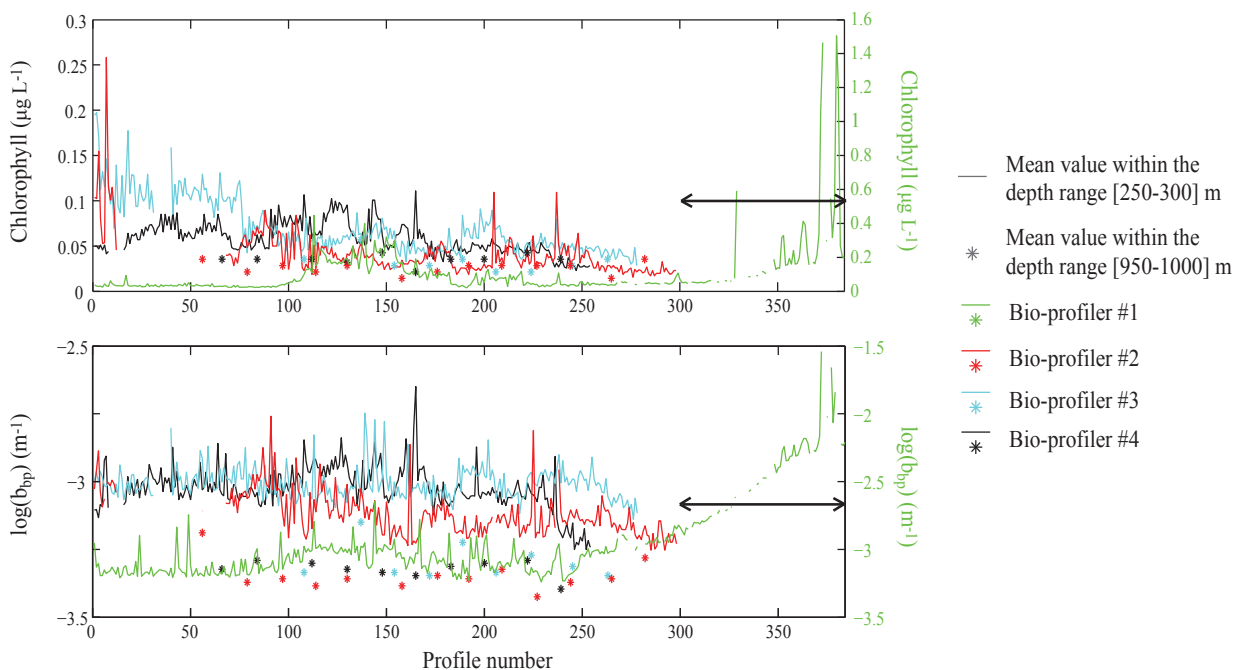
1453 ^a Subsurface values exceeding surface values by more than 60%

1454 ^b Subsurface values exceeding surface values by more than 100%

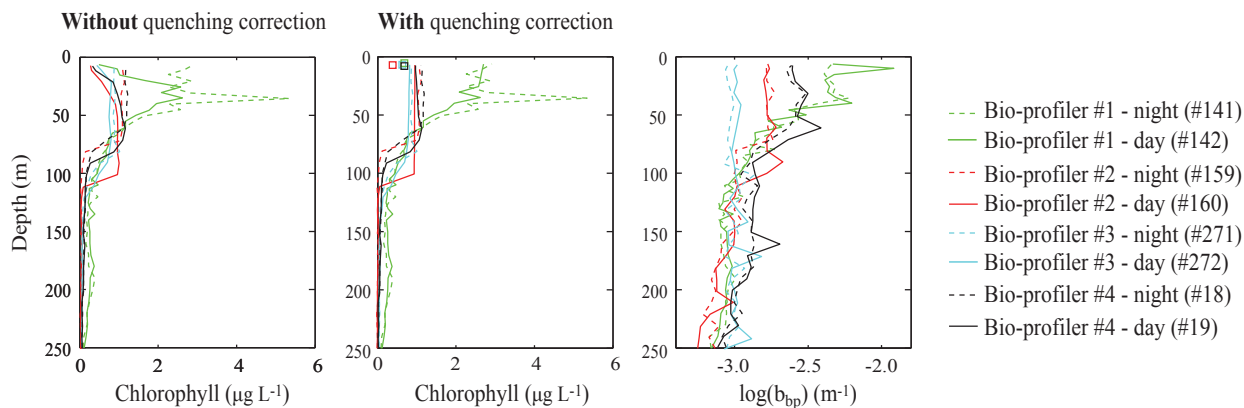
1455 ^c For some corrected profiles, a large decrease of the chlorophyll concentration still occurred in the
 1456 surface layer. These profiles were flagged in Figures 2b (squares), 4 (squares) and 5 (red circles).
 1457 See the method section and the caption of Figure 2b for more details.



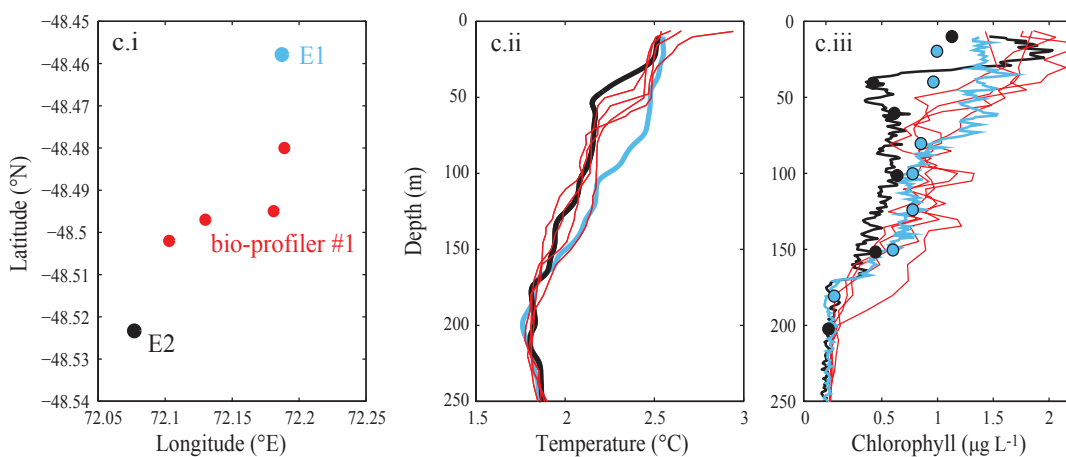
a) Drifting assessment

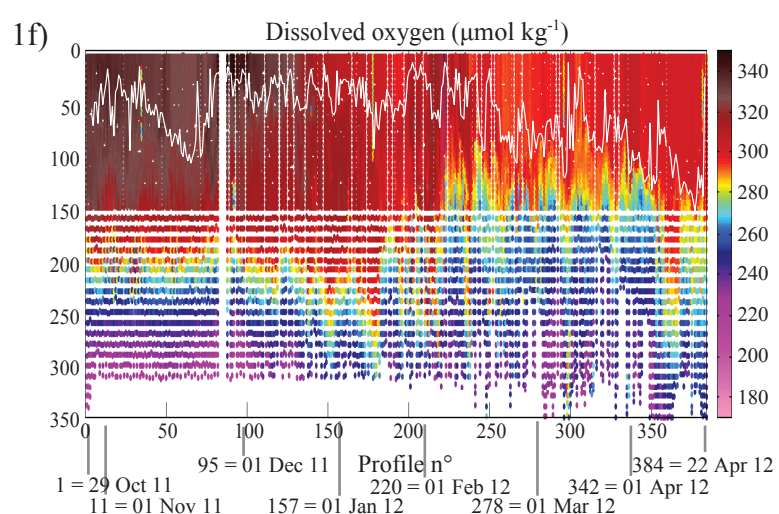
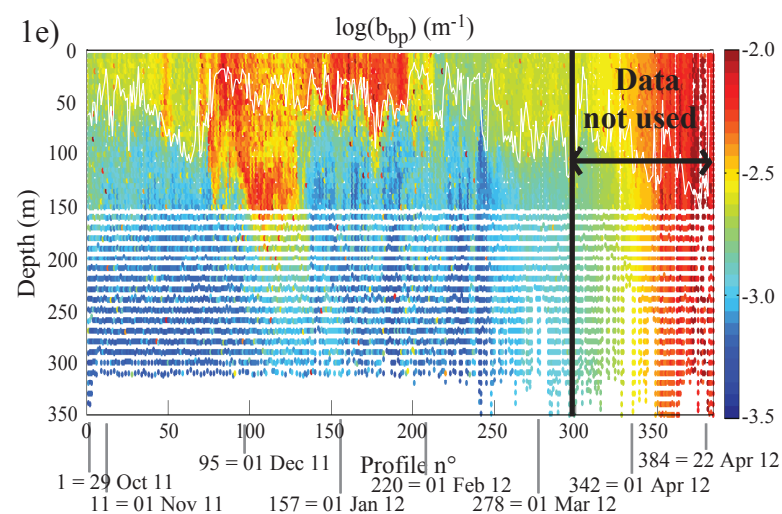
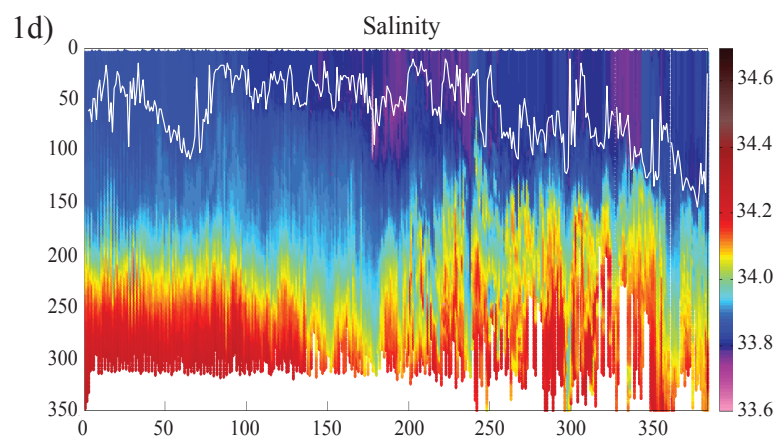
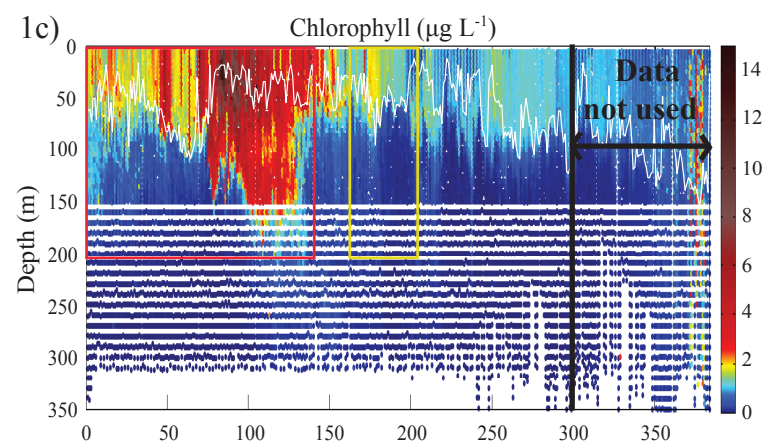
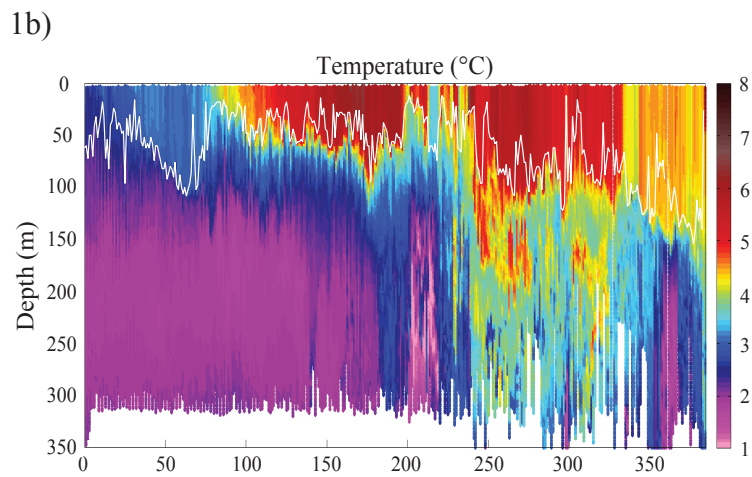
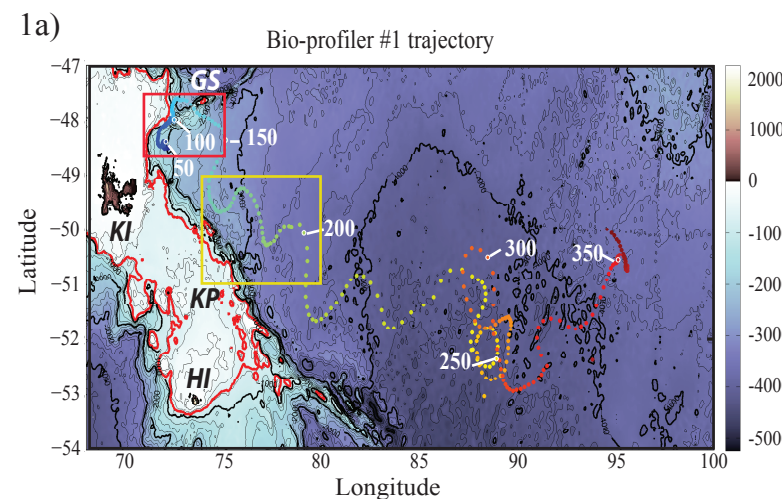


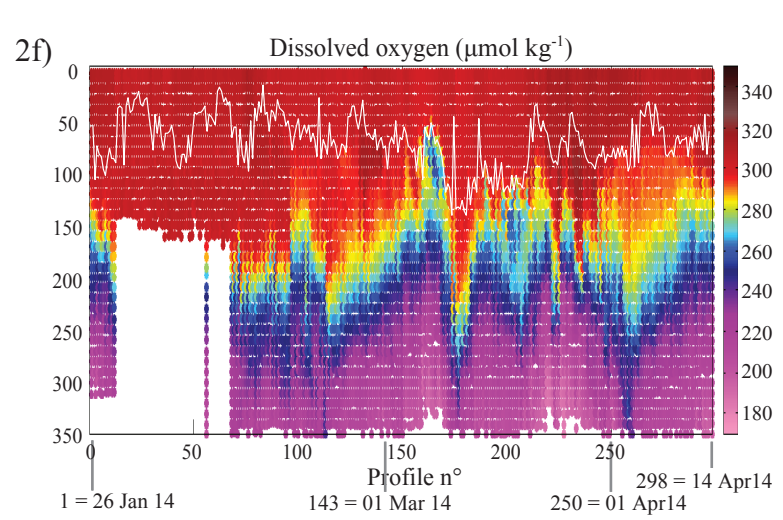
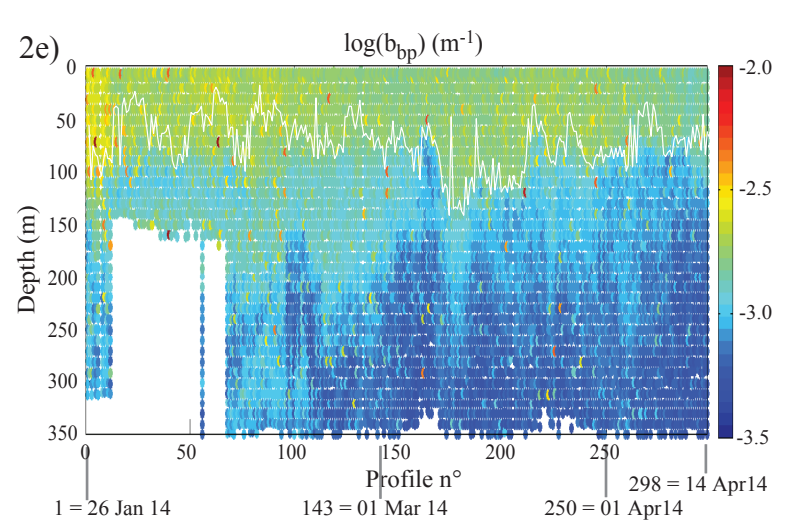
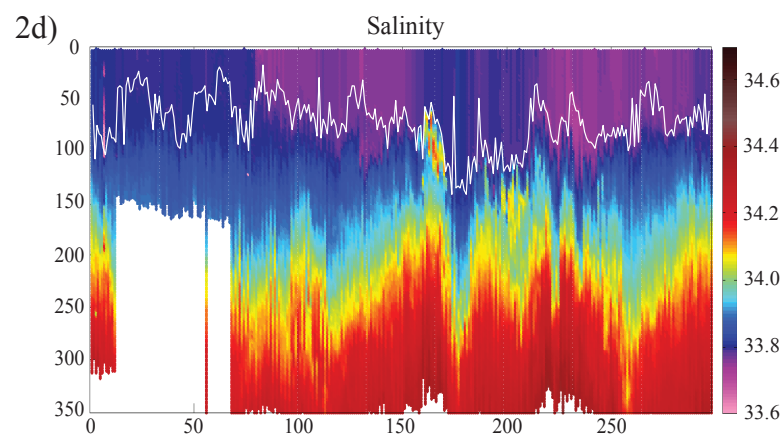
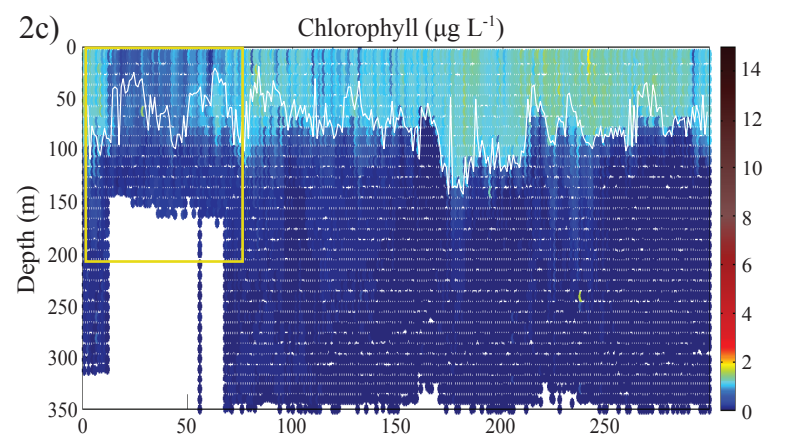
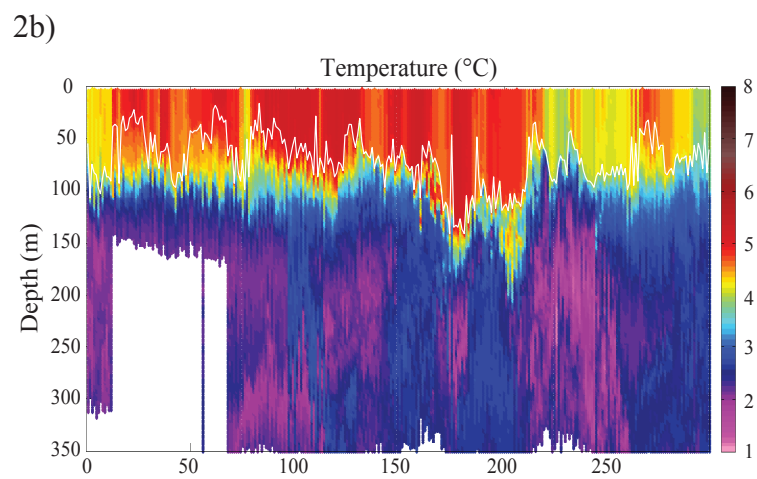
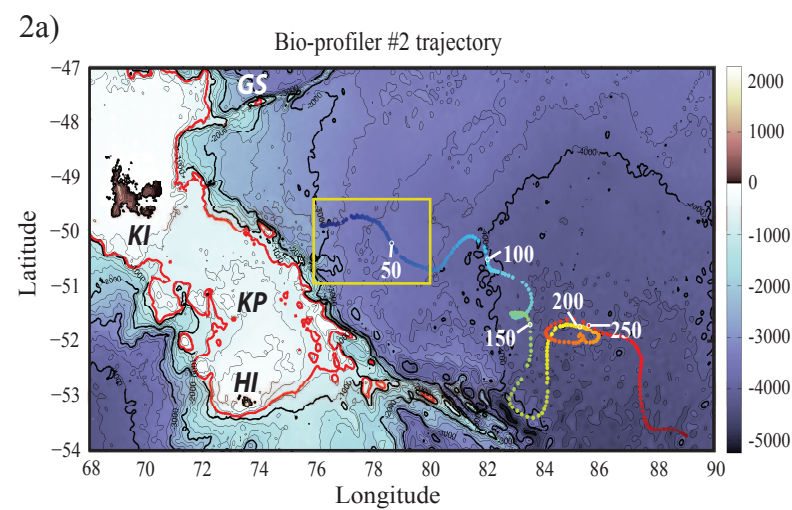
b) Quenching assessment

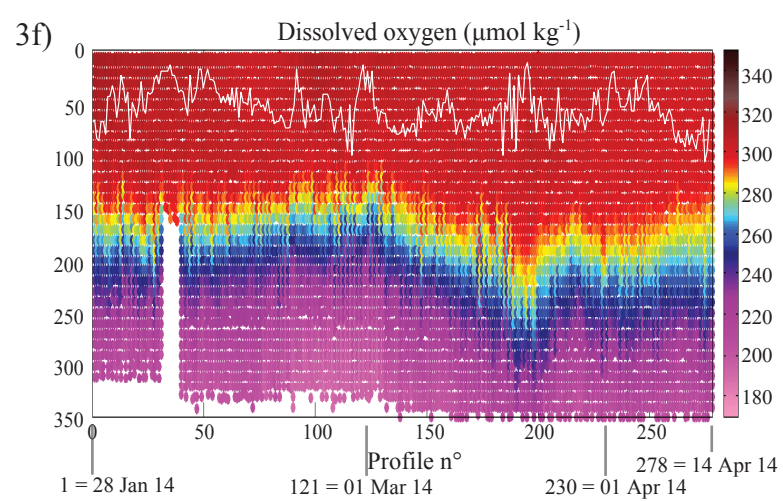
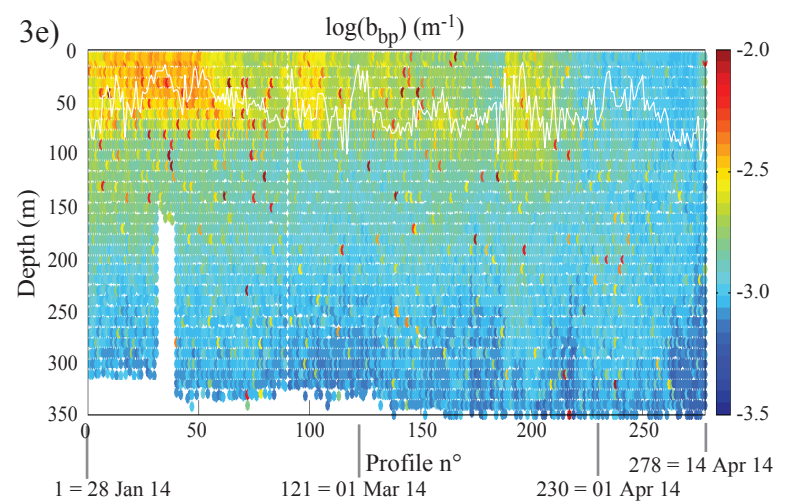
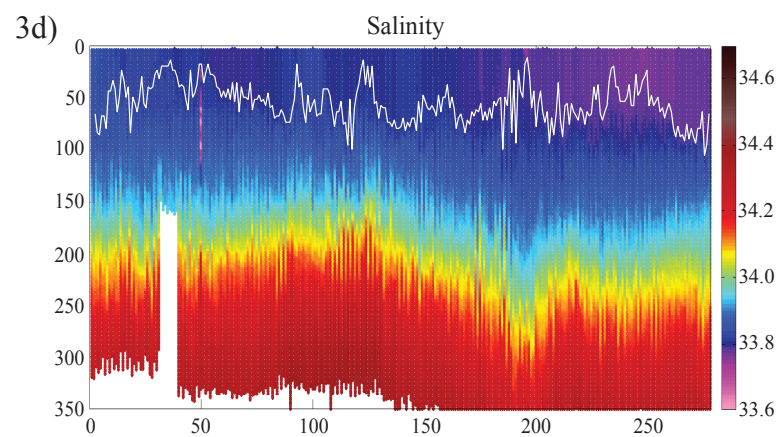
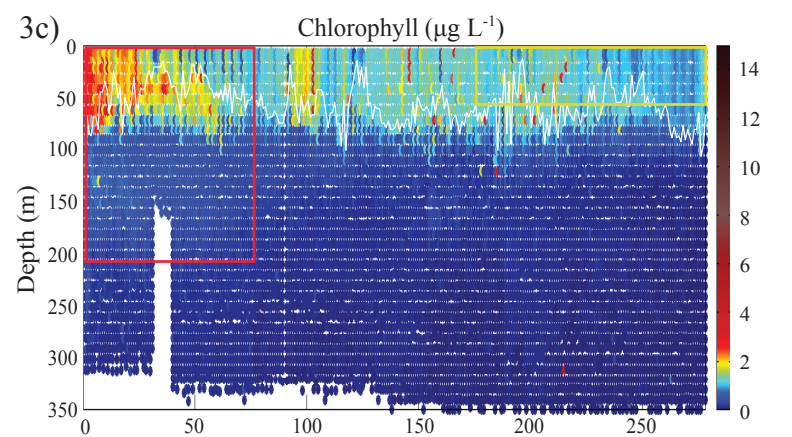
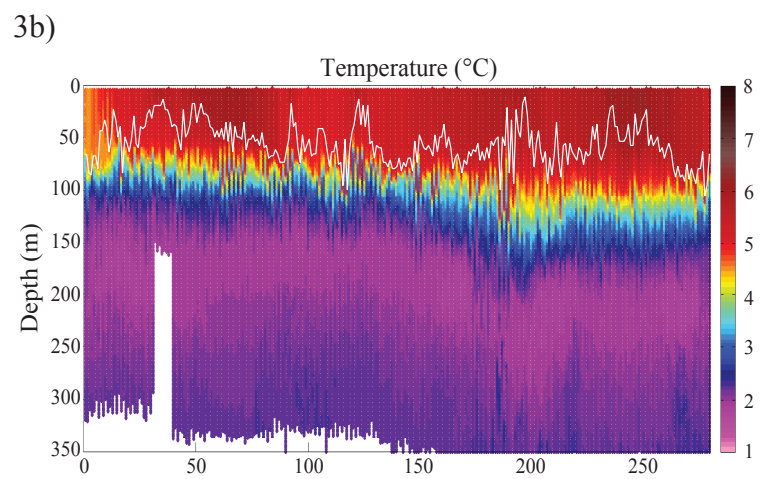
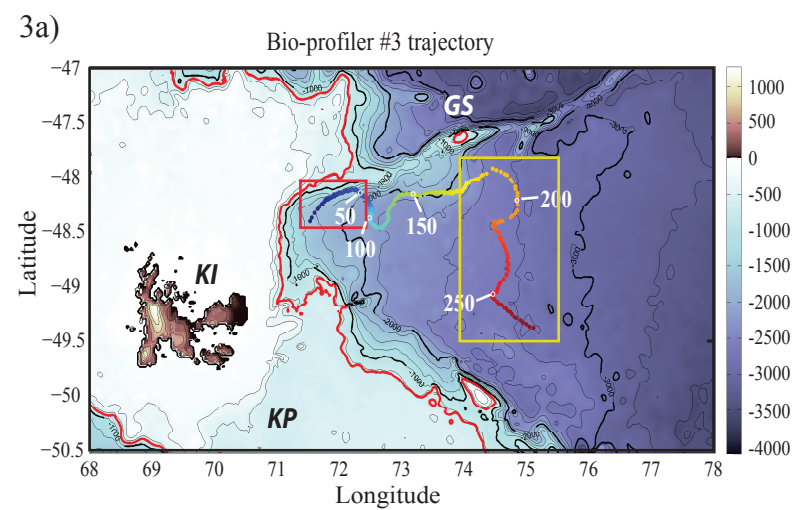


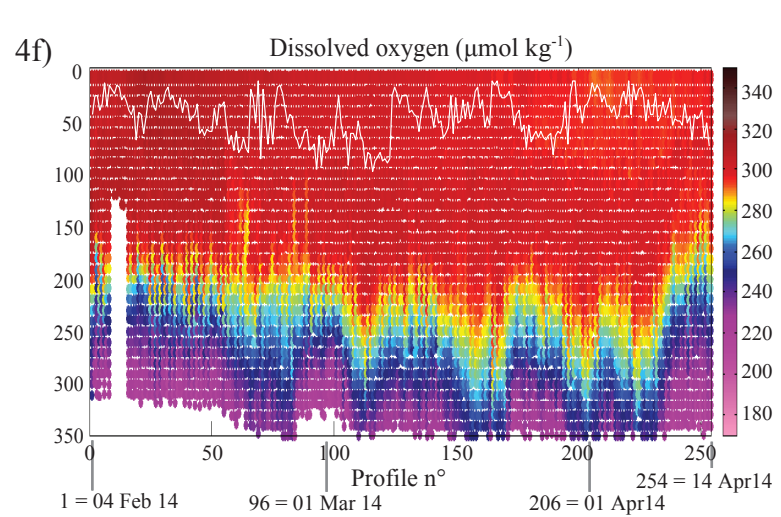
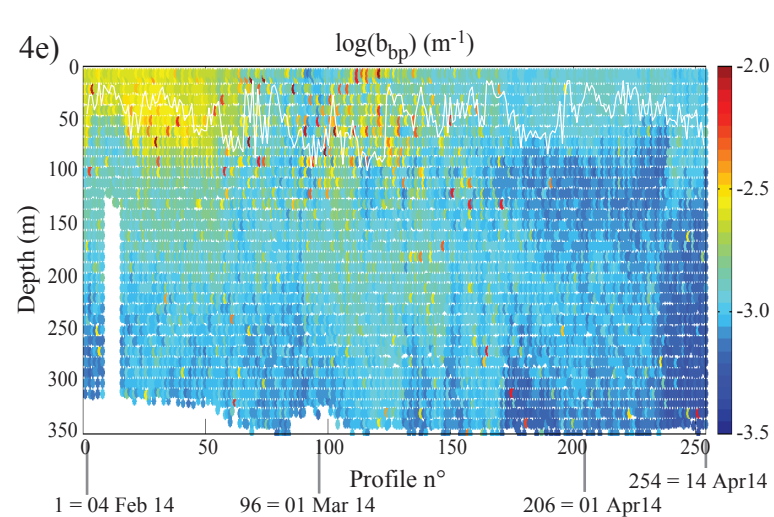
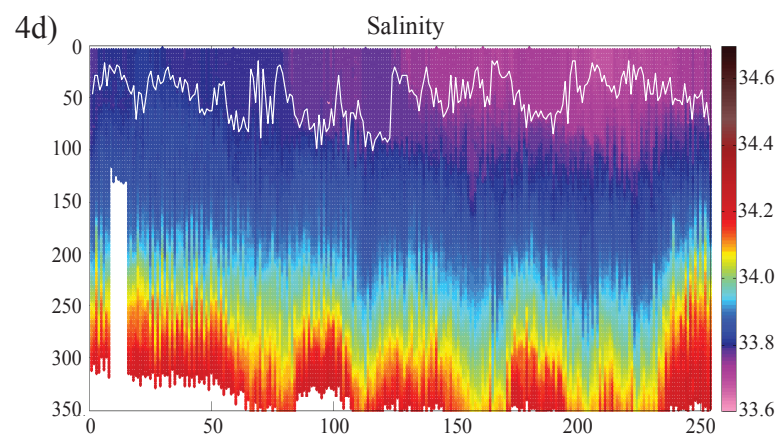
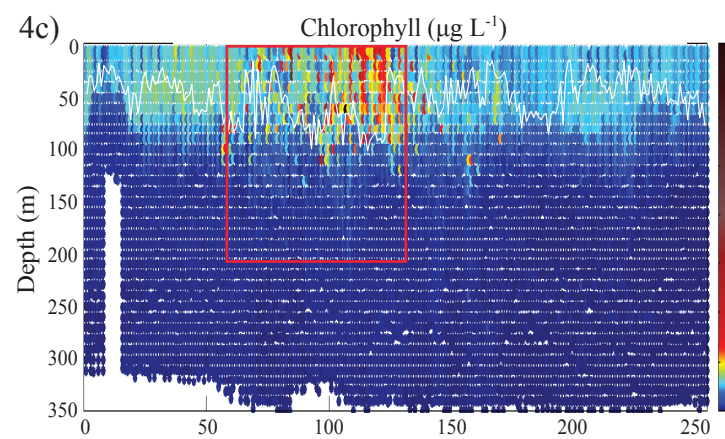
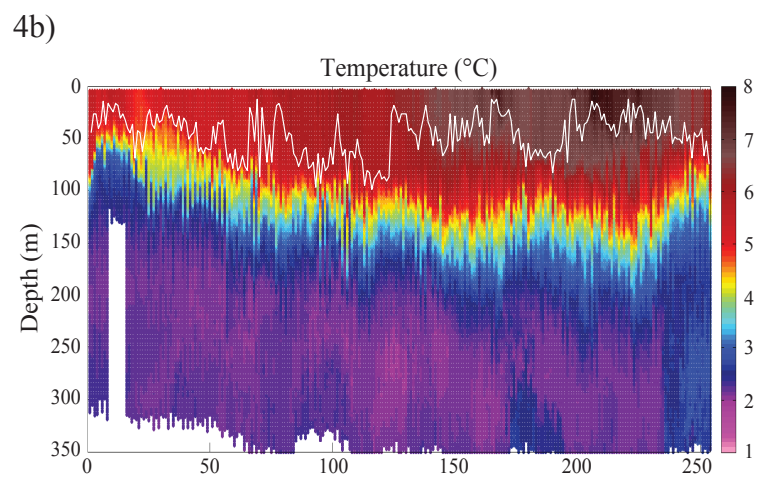
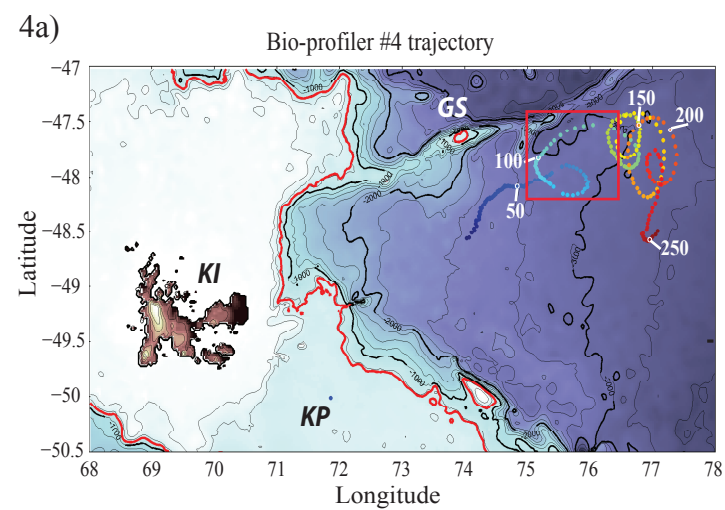
c) Comparison to KEOPS2 shipboard observations



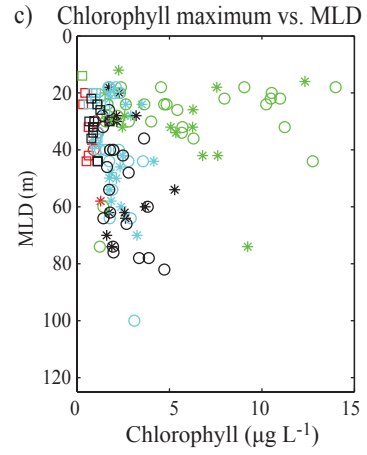
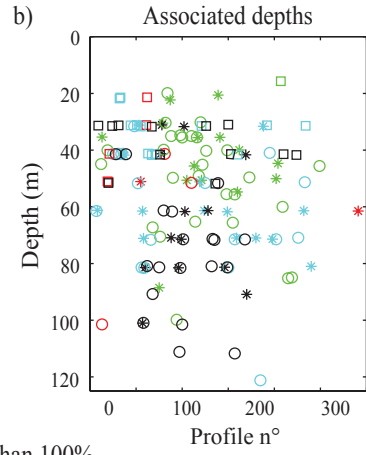
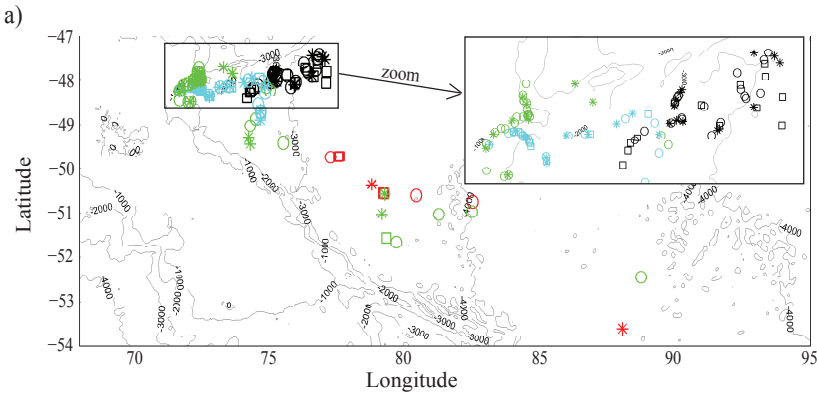




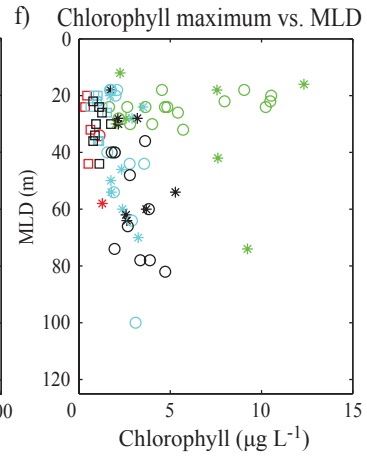
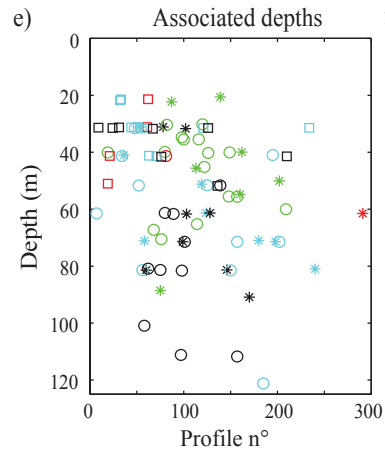
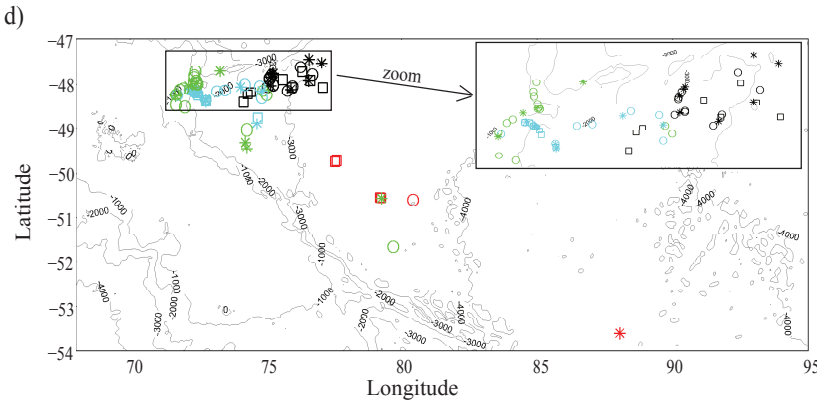


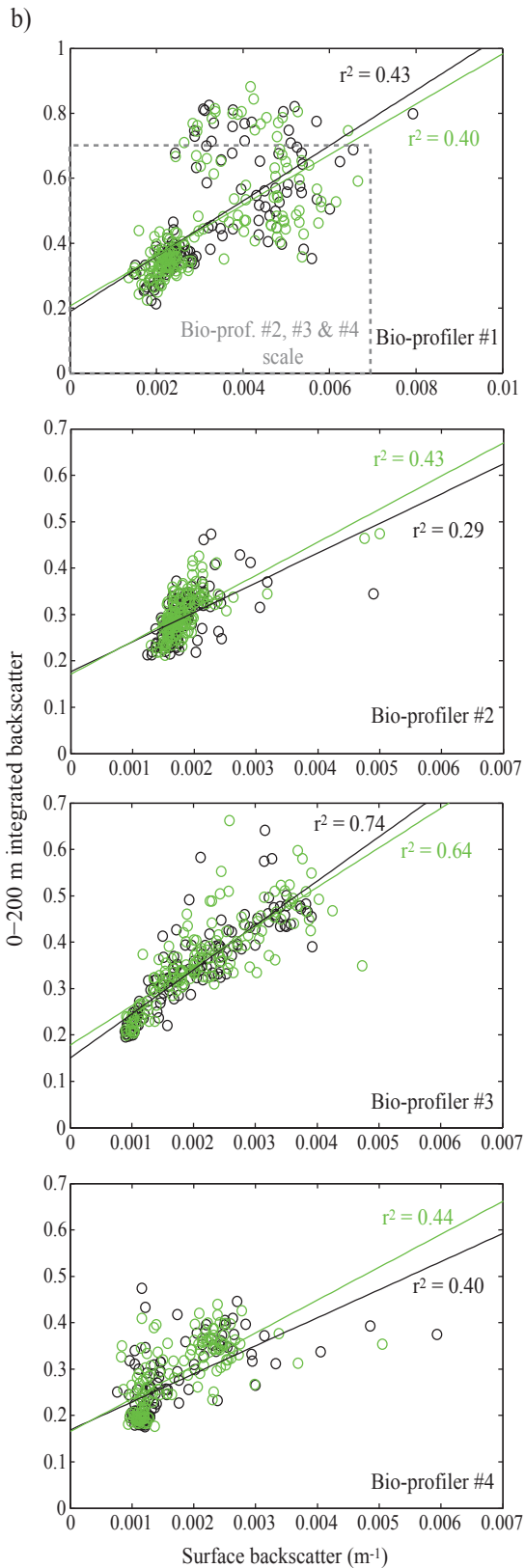
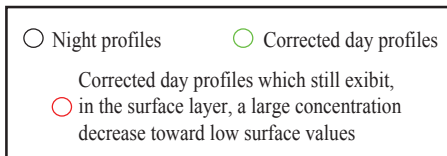
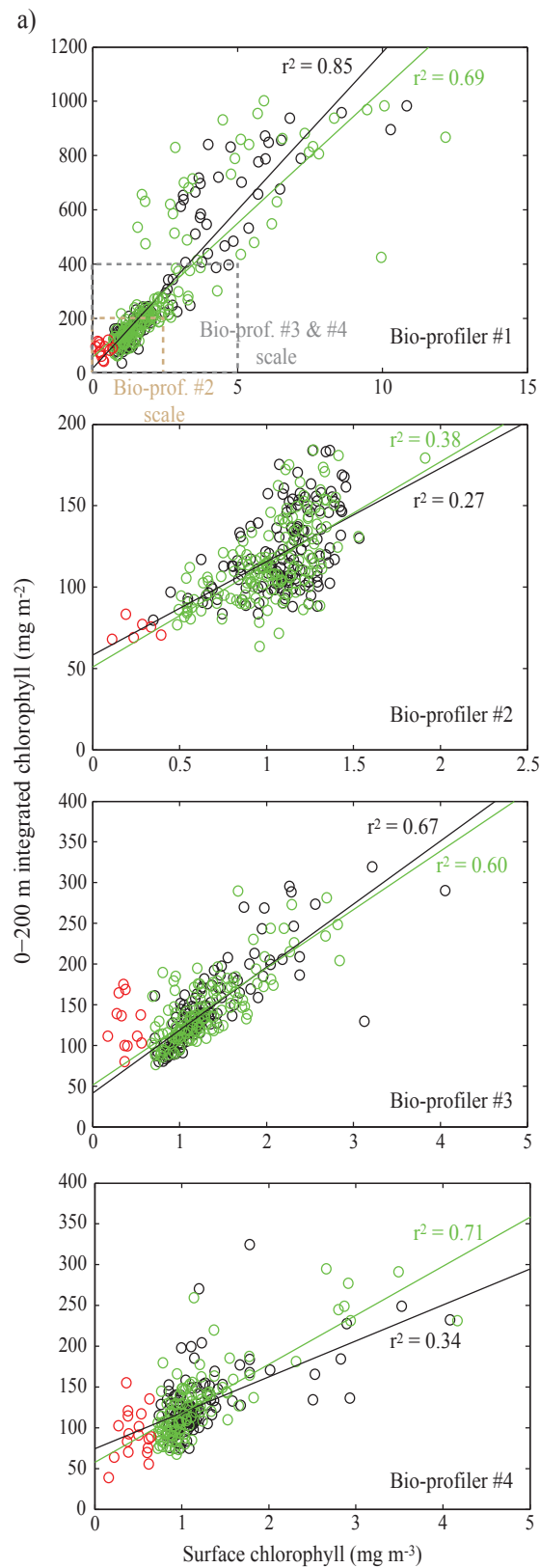


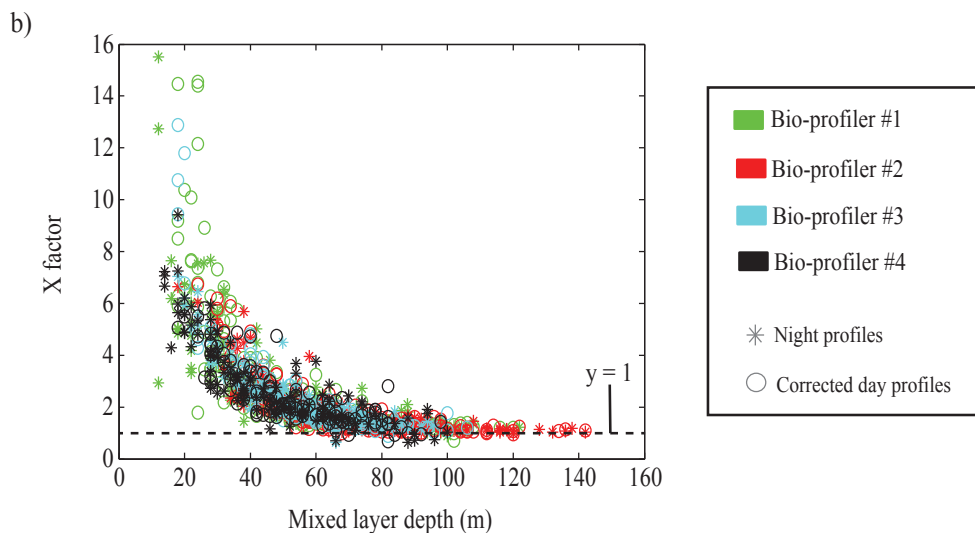
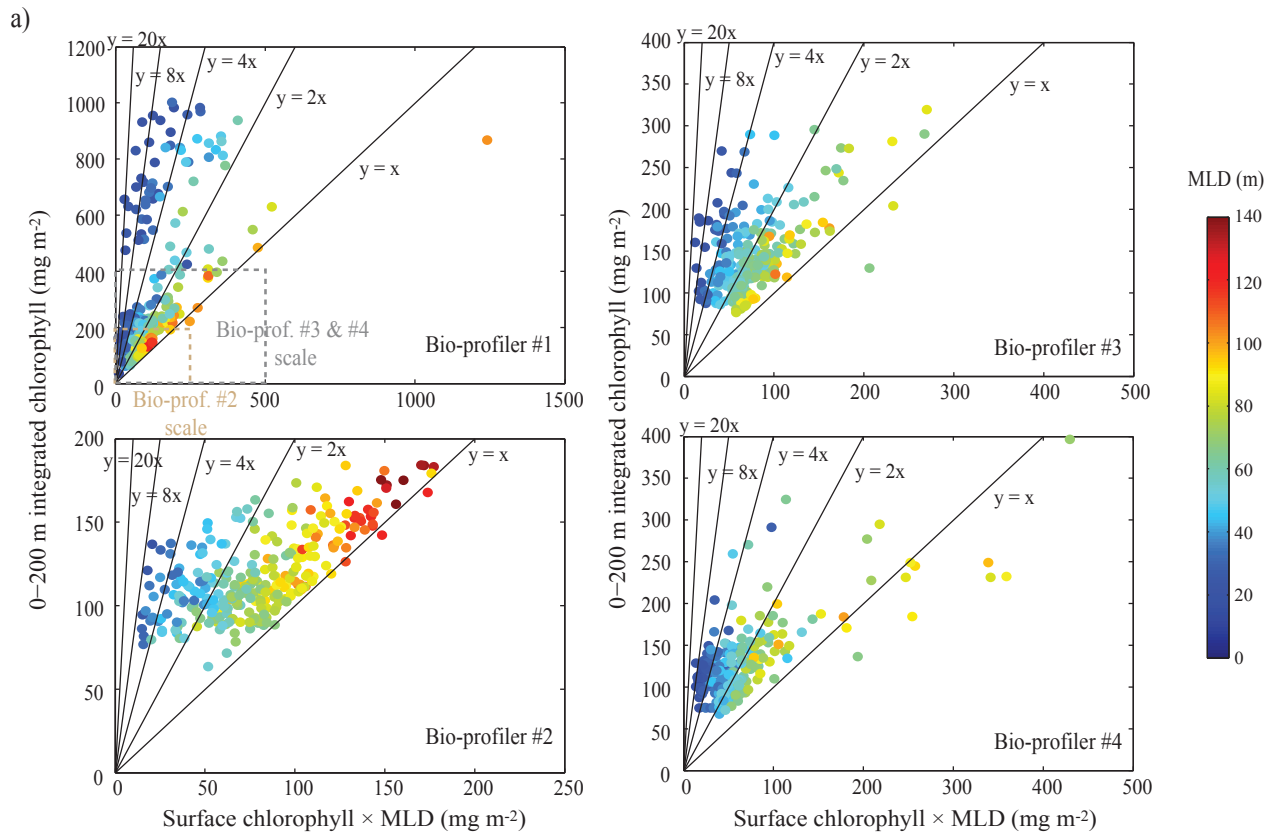
Areas where subsurface chlorophyll maximum exceeds the surface content of more than 60%



Areas where subsurface chlorophyll maximum exceeds the surface content of more than 100%

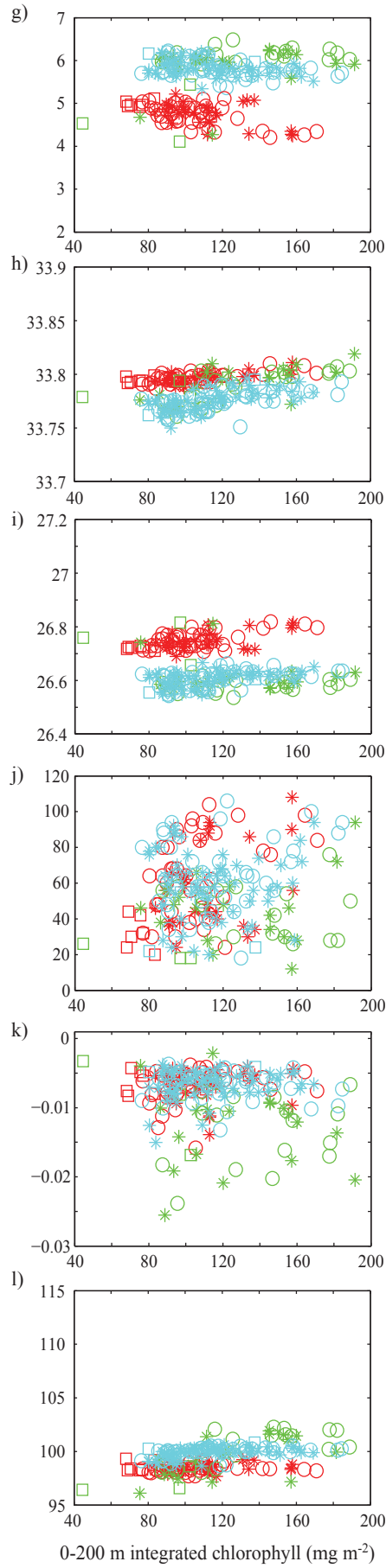
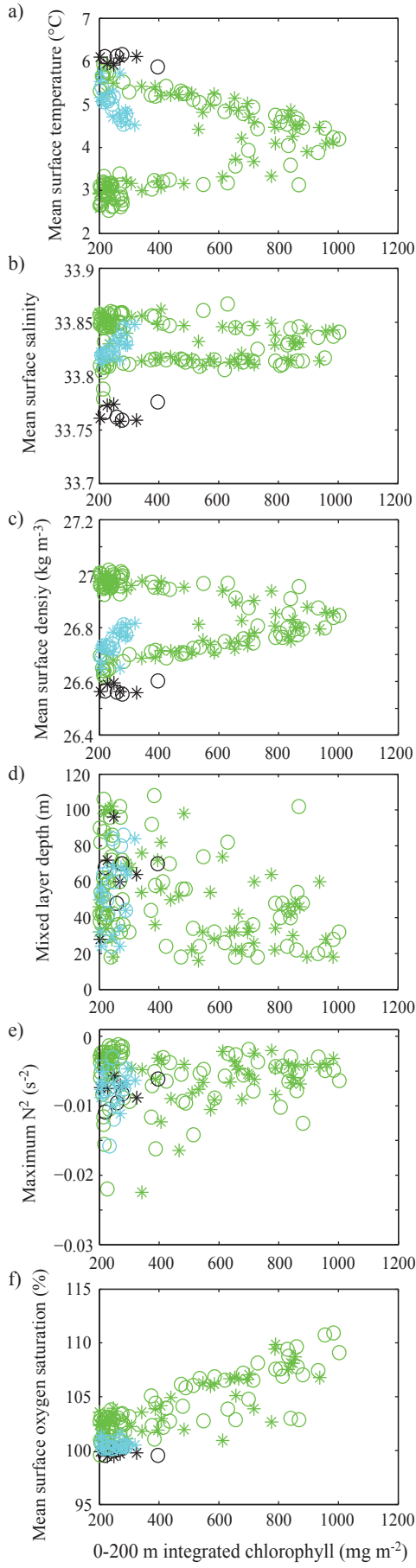






Rich biomass regions

Moderate biomass regions



■ Bio-profiler #1
 ■ Bio-profiler #2
 ■ Bio-profiler #3
 ■ Bio-profiler #4

* Night profiles
 ○ Corrected day profiles

□ Corrected day profiles which still exhibit, in the surface layer, a large concentration decrease toward low surface values

